MOX-Report No. 03/2017

On a free-surface problem with moving contact line: from variational principles to stable numerical approximations

Fumagalli, I.; Parolini, N.; Verani, M.

MOX, Dipartimento di Matematica
Politecnico di Milano, Via Bonardi 9 - 20133 Milano (Italy)

mox-dmat@polimi.it http://mox.polimi.it

On a free-surface problem with moving contact line: from variational principles to stable numerical approximations

Ivan Fumagalli[a,*], Nicola Parolini[a], Marco Verani[a]

[a] *MOX, Dipartimento di Matematica, Politecnico di Milano, P.za Leonardo da Vinci 32, 20133 Milano, Italy*

Abstract

We analyze a free-surface problem described by time-dependent Navier-Stokes equations. Surface tension, capillary effects and wall friction are taken into account in the evolution of the system, influencing the motion of the contact line – where the free surface hits the wall – and of the dynamics of the contact angle. The differential equations governing the phenomenon are first derived from the variational principle of minimum reduced dissipation, and then discretized by means of the ALE approach. The numerical properties of the resulting scheme are investigated, drawing a parallel with the physical properties holding at the continuous level. Some instability issues are addressed in detail, in the case of an explicit treatment of the geometry, and novel additional terms are introduced in the discrete formulation in order to damp the instabilities. Numerical tests assess the suitability of the approach, the influence of the parameters, and the effectiveness of the new stabilizing terms.

Keywords: capillary, Geometric Conservation Law, Arbitrary Lagrangian-Eulerian, generalized Navier boundary condition, contact angle

1. Introduction

The simulation of free-boundary problems is of major relevance in many fluid-dynamics applications, both at the large scale, like in the study of water waves [1] and the design of watercraft [2], and at the microscopic scale, e.g. in the microfluidics of capillary tubes [3, 4] or labs-on-a-chip [5, 6]. In these settings, the fluid under inspection interacts with other fluids or solids, and thus it is fundamental to correctly track the evolution of the interfaces between the different phases. Different approaches can be found, in the literature, for the modeling and the simulation of multiphase problems, and they can be classified in three main categories, depending on their treatment of the interfaces: the diffuse-interface models, the interface-capturing methods and the interface-tracking techniques. The phase-field model [7, 8, 5] is representative of the first category: regions occupied by different phases are identified by different integer values of a scalar function, and the interface has a finite thickness, spanning the region where this function smoothly passes from a level to another. This kind of smoothing of the interface allow an accurate physical characterization (including phase transitions) and helps in the development and the proof of theoretical results, but does not provide a sharp position of the interface. On the other hand, in interface-capturing methods, like the level-set method [9, 10] or the volume-of-fluid method [11, 12], a precise description of the interface is given at any time, as a codimension-1 manifold immersed in the domain. However, these methods require the solution of both the fluid phases separated by the interface, and at the discrete level it is crucial to properly handle the elements of the computational domain through which the interface passes, since the grid is not conforming to the interface. Eventually, the third category of methods includes the techniques to track the

*Corresponding author

Email addresses: ivan.fumagalli@polimi.it (Ivan Fumagalli), nicola.parolini@polimi.it (Nicola Parolini), marco.verani@polimi.it (Marco Verani)

interface as an actual boundary of the domain, which is thus moved accordingly. The computation of the domain motion is a major point of these techniques, and the Arbitrary Lagrangian-Eulerian approach (ALE) [13, 14] is widely adopted to this aim. Since the interface is not immersed in the domain, in many cases one can actually restrict the computational domain to a single phase of interest.

When more than two phases simultaneously interact, particular attention has to be paid to triple lines, where different interfaces intersect. Indeed, the overall evolution of the system is highly influenced by the physical relations occurring on these lines. In case one of the phases under consideration is a solid, the triple line is called the *contact line*, and if a naïve approach is adopted, one may draw paradoxical conclusions on the physical laws holding thereat. This issue is known as the moving-contact-line problem, and it has been addressed in various ways, in the literature (see, e.g., [15, 6, 16, 17]).

In the present work, we analyze a free-surface problem for a Newtonian fluid inside a capillary tube, described by time-dependent, incompressible Navier-Stokes equations and discretized via the Finite Element method (FEM), with an ALE approach accounting fro the domain motion. At the free surface, the interaction with a gas is included by means of a surface-tension condition, connecting the curvature of the interface and the stress exchanged between the fluids. The effects of wall friction and contact line forces are gathered in the generalized Navier boundary condition (GNBC), imposed on the solid wall. This condition includes the imposition of an equilibrium *contact angle*, that is the angle between the free surface and the wall. Such an angle is a primary feature of the shape of capillary menisci and resting droplets, and its imposition by the GNBC has been widely adopted and motivated in the literature of the last decade [15, 17, 6].

The goal of this work is to investigate the properties of the discretization of the problem under inspection, and to propose a solution to possible stability issues. To this aim, we deeply inspect the structure of the problem, starting from the derivation of the equations at hand from the physical variational principles governing it. This variational approach is shared by other works that can be found in the literature (see, e.g., [18, 19]). Our contribution in this regard is the employment and a mild generalization of the Principle of minimum reduced dissipation [20], which represents a general framework for the derivation of differential problems, without resorting to any microscopical consideration. Keeping a parallel between the discrete settings and the laws holding at the continuous level, we will be able to identify the possible sources of instability, in the numerical scheme, and to propose a strategy to control them. This represents a novelty with respect to the results obtained in [15].

The present paper is organized as follows. In Sec. 2, the physical phenomenon under inspection is presented, together with the equations governing it. Domain motion is then addressed, and some shape calculus definitions and results are stated. Then, in Sec. 3, the differential problem describing the system is derived from physical variational principles, considering both the case of a closed system, and the possibility of mass exchanges with the environment. Sec. 4 is devoted to the weak formulation of the problem and to its ALE-FEM discretization. The numerical properties of the resulting scheme are investigated in Sec. 5, in light of the results of Sec. 3. Some stability issues are addressed in detail, in the case of an explicit treatment of the geometry, and a novel stabilization term is introduced. In Sec. 6, several tests assess the suitability of the numerical scheme in reproducting the physical phenomena under consideration. Time and space discretization are inspected, and their influence on the physical parameters of the model is examined. Experimental data, taken from [4], are then employed to validate the numerical scheme. Finally, the effectiveness of the proposed stabilization technique is verified.

2. Preliminaries

We consider a fluid contained in a region $\Omega \subset \mathbb{R}^d$, $d = 2, 3$, as depicted in Fig. 1. The edge Σ_b is a virtual boundary separating the domain Ω from the rest of the space occupied by the fluid, thus energy and mass exchanges can occur through it. A solid wall is on the lateral side of the domain, and we denote by Σ the part of the wall that is wetted by the fluid at hand, and by Σ_g the remaining part, in contact with an other fluid, that we assume to be a gas. This gas is separated from the region Ω by the free surface Γ, and we are not interested in studying the gaseous phase, unless for the influence that its presence has on the fluid contained in Ω. The contact line where the three phases meet is denoted by $\partial\Gamma = \overline{\Gamma} \cap \overline{\Sigma}$. The tangent vector of the line $\partial\Gamma$ is denoted by $\boldsymbol{\tau}_{\partial\Gamma}$ and we denote by $\mathbf{b}$ and $\mathbf{b}_s$ the unit vectors that are normal to the

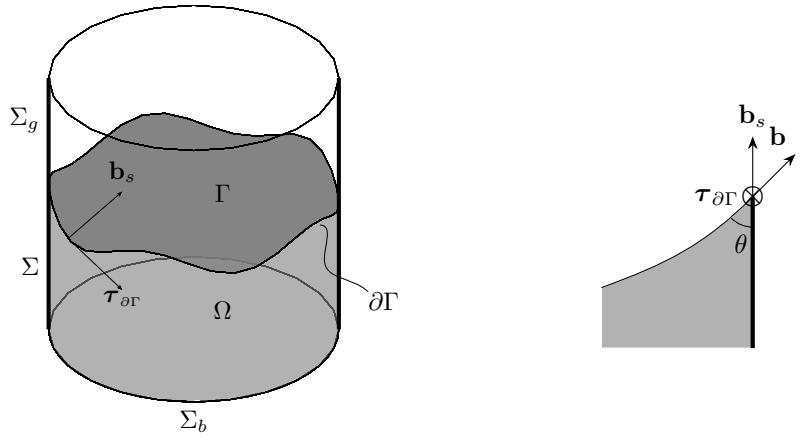

Figure 1: Domain and geometric notation. On the right, a zoom near the contact line, in a plane orthogonal to $\boldsymbol{\tau}_{\partial\Gamma}$.

$\boldsymbol{\tau}_{\partial\Gamma}$ and aligned along the free surface Γ and the wall Σ, respectively (cf. Fig. 1, right). On the contact line, we introduce also the function $\theta : \partial\Gamma \to \mathbb{R}$ denoting the corresponding contact angle, that is such that $\cos\theta = \mathbf{b} \cdot \mathbf{b}_s$.

The domain at time t is denoted by Ω^t and it is identified as the image of an initial domain $\Omega^0 = \Omega$ through a map $\mathcal{A}_t : \Omega \to \mathbb{R}^d$. A similar notation will be used for all the other quantities, in the rest of the paper: the superscript t indicates that the quantity is taken at time t. Assuming the family $\mathcal{A}_t$ of maps to be smooth w.r.t. time, and each map invertible, we can define the Lagrangian and Eulerian domain velocity fields as

$$\begin{aligned} \widehat{\mathbf{V}}(t, \widehat{\mathbf{x}}) &= \partial_t \mathcal{A}_t(\widehat{\mathbf{x}}), \qquad && \forall \widehat{\mathbf{x}} \in \Omega, \\ \mathbf{V}(t, \mathbf{x}) &= \widehat{\mathbf{V}}(t, \mathcal{A}_t^{-1}(\mathbf{x})), \qquad && \forall \mathbf{x} \in \Omega^t, \end{aligned} \tag{1}$$

respectively. Being the wall Σ^t impervious, and wanting to keep Σ_b fixed, at each time t the domain velocity field $\mathbf{V}(t, \cdot)$ has to belong to the admissible set

$$\mathcal{U}_{ad} = \left\{ \mathbf{v} : \Omega^t \to \mathbb{R}^d \mid \quad \mathbf{v} \cdot \boldsymbol{\nu} = 0 \text{ on } \Sigma^t, \quad \mathbf{v} = \mathbf{0} \text{ on } \Sigma_b \right\}.$$

In the definition above, and throughout the paper, by $\boldsymbol{\nu}$ we denote the normal vector defined almost everywhere on $\partial\Omega^t$. Indeed, for our purposes, we will not need a univocal definition of $\boldsymbol{\nu}$ on the zero-measure lines $\partial\Gamma^t$ and $\overline{\Sigma^t} \cap \overline{\Sigma}_b$.

Remark 1 (Shape kinematics). We point out that the actual evolution of the domain is governed by the sole normal component $\mathbf{V} \cdot \boldsymbol{\nu}$ of the domain velocity, at the boundary $\partial\Omega^t$ of the domain. Therefore, any variation of the tangential components or of the bulk distribution, that leaves $\mathbf{V} \cdot \boldsymbol{\nu}$ unaffected, does not impact on the domain evolution, whence some freedom is left in the definition of $\mathbf{V}$. This freedom will be exploited in the numerical formulation of the free boundary problem.

Assuming immiscibility between the different phases involved in the physical system, and neglecting phase transitions, the motion of the free surface Γ^t follows the movement of the particles of the fluid occupying Ω^t. Hence, according to Remark 1, the geometrical velocity $\mathbf{V}$ and the Eulerian velocity $\mathbf{u}$ of the fluid are coupled by [1]

$$\mathbf{V} \cdot \boldsymbol{\nu} = \mathbf{u} \cdot \boldsymbol{\nu} \qquad \text{on } \Gamma^t. \tag{2}$$

Moreover, the fluid in Ω^t is assumed to be Newtonian and incompressible, and the forces acting on it are gravity, surface tension, and a possible external stress imposed at the open edge Σ_b. Hence, supposing

[1] For ease of notation, from now on we omit the explicit dependence on time or space, where no misunderstanding is possible.

to know the initial configuration Ω and fluid velocity field $\mathbf{u}^0$, the state of the flow at time t is described by the current domain Ω^t, the fluid Eulerian velocity $\mathbf{u}$ and the pressure p. We remark that, thanks to incompressibility, we can consider the rescaled pressure $p = \widetilde{p}/\rho$, that is the ratio between the physical pressure $\widetilde{p}$ and the fluid density ρ. Analogously, the kinematic viscosity $\nu = \mu/\rho$ is going to appear in the differential model, in place of the dynamic viscosity μ. The state problem, solved by the couple $(\mathbf{u}, p)$ at time t is, then, the following:

$$\begin{cases} \partial_t \mathbf{u} + (\mathbf{u}\cdot\nabla)\mathbf{u} - \operatorname{div}\sigma = \mathbf{g} & \text{in } \Omega^t, t>0, \\ \operatorname{div}\mathbf{u} = 0 & \text{in } \Omega^t, t>0, \\ \sigma\boldsymbol{\nu}\cdot\boldsymbol{\tau} = 0, \quad \sigma\boldsymbol{\nu}\cdot\boldsymbol{\nu} + \gamma H = 0 & \text{on } \Gamma^t, t>0, \quad \forall \boldsymbol{\tau}\perp\boldsymbol{\nu}, \\ \mathbf{u}\cdot\boldsymbol{\nu} = \mathbf{V}\cdot\boldsymbol{\nu} & \text{on } \Gamma^t, t>0, \\ \mathbf{u}\cdot\boldsymbol{\nu} = 0, \quad (\sigma\boldsymbol{\nu} + \beta\mathbf{u} + \gamma(\cos\theta - \cos\theta_s)\delta_{\partial\Gamma}\,\mathbf{b}_s)\cdot\boldsymbol{\tau} = 0 & \text{on } \Sigma^t, t>0, \quad \forall \boldsymbol{\tau}\perp\boldsymbol{\nu}, \\ \sigma\boldsymbol{\nu} = \boldsymbol{\zeta} & \text{on } \Sigma_b, t>0, \\ \mathbf{u} = \mathbf{u}^0 & \text{in } \Omega^0, t=0, \end{cases} \tag{3}$$

where $\sigma = \nu\left(\nabla\mathbf{u} + \nabla\mathbf{u}^T\right) - pI$ is the stress tensor, I being the identity tensor, $\mathbf{g} = -g\mathbf{e}_d$ is the gravity force, $\mathbf{e}_d$ being the upwards vertical vector of the canonical basis $\{\mathbf{e}_i\}_{i=1}^d$, γ is the surface tension coefficient on Γ^t, H is the total curvature of Γ^t, β is the friction coefficient on Σ^t, and $\boldsymbol{\zeta}$ is an external stress applied on Σ_b. The distribution $\delta_{\partial\Gamma}$ is defined as

$$\langle \delta_{\partial\Gamma}, \varphi\rangle = \int_{\partial\Gamma^t} \varphi\, d\lambda, \qquad \text{for any smooth function } \varphi,$$

with λ denoting the $(d-2)-$dimensional Lebesgue measure on $\partial\Gamma^t$. [2] We notice that the equations depend both on the current value of the time-dependent contact angle θ and on its static value θ_s. The latter is defined in terms of the material properties of the three phases interacting around the contact line, through the Young equation [21]

$$\gamma\cos\theta_s + \gamma_l - \gamma_g = 0, \tag{4}$$

where γ_l and γ_g are the surface tension coefficients on Σ^t and Σ_g^t, respectively. The discrepancy of the dynamic contact angle θ from θ_s induces the *uncompensated Young stress*

$$\gamma(\cos\theta - \cos\theta_s)\tau\cdot\mathbf{b}_s\,\delta_{\partial\Gamma},$$

a force which is concentrated on the contact line and oriented along the wall in the normal direction $\mathbf{b}_s$ to $\partial\Gamma^t$ (an upwards vertical force for $d=2$). This force is responsible for the formation of the meniscus in capillary tubes [21], as we will see in the numerical results of Sec. 6.

The equations (3) can be derived from physical principles, in particular employing the Principle of minimum reduced dissipation [20]. We are going to devote Sec. 3 to this topic, but we want to mention since now that this derivation is prompted by a suitable formulation of the First Law of Thermodynamics, which reads

$$\mathcal{W} = 2\mathcal{R}, \tag{5}$$

where $\mathcal{W}$ is the total power of the external forces, of the form

$$\mathcal{W} = \int_{\Omega^t} \mathbf{B}\cdot\mathbf{u} + \int_{\partial\Omega^t} \mathbf{T}\cdot\mathbf{u},$$

for suitable choices of the generalized forces $\mathbf{B} = \mathbf{B}\left(\mathbf{g}, \rho, \widetilde{p}, \mathbf{u}\right), \mathbf{T} = \mathbf{T}(\boldsymbol{\zeta}, \mathbf{g}, \rho, \gamma, \theta_s, \theta, H, \widetilde{p})$, whereas $\mathcal{R}$ is the Rayleigh dissipation function, defined as

$$\mathcal{R} = \frac{1}{2}\int_{\Omega^t} 2\mu|D(\mathbf{u})|^2 + \frac{1}{2}\int_{\Sigma^t} \widetilde{\beta}|\mathbf{u} - \mathbf{u}\cdot\boldsymbol{\nu}\,\boldsymbol{\nu}|^2, \tag{6}$$

[2] In the rest of the paper, Lebesgue measure of any dimension will be understood in all the integrals.

with $D(\mathbf{u}) = \frac{1}{2}\left(\nabla\mathbf{u} + \nabla\mathbf{u}^T\right)$ being the strain tensor of the fluid. This law is a fundamental relation governing the physics of the phenomenon, and its discrete counterpart will be explored in Sec. 5. In order to actually perform the hinted derivation, we need some technical tools, that we collect hereafter.

2.1. Technical tools

In this section, we recall some useful definitions and results that will be employed in the rest of the paper. Herein, Γ denotes a generic smooth hypersurface of dimension $d-1$, for simplicity immersed in $\mathbb{R}^d$, and $\partial\Gamma$ indicates its boundary. The *tangential gradients* of a scalar differentiable function $\psi : \Gamma \to \mathbb{R}$ and a vectorial differentiable function $\boldsymbol{\psi} : \Gamma \to \mathbb{R}^d$ are defined via the projector $\Pi_\Gamma = I - \boldsymbol{\nu} \otimes \boldsymbol{\nu}$:

$$\nabla_\Gamma \psi = \Pi_\Gamma \nabla\psi, \qquad \nabla_\Gamma \boldsymbol{\psi} = \left(\nabla\boldsymbol{\psi}\,\Pi_\Gamma\right)^T = \nabla\boldsymbol{\psi}\,\Pi_\Gamma.$$

Accordingly, the *tangential divergence* of $\boldsymbol{\psi}$ reads

$$\operatorname{div}_\Gamma \boldsymbol{\psi} = \operatorname{tr} \nabla_\Gamma \boldsymbol{\psi} = \Pi_\Gamma \cdot \nabla\boldsymbol{\psi}.$$

It is possible to prove [22] that the total curvature H of Γ is related to its normal vector $\boldsymbol{\nu}$ by

$$\operatorname{div}_\Gamma \boldsymbol{\nu} = H,$$

whence the following integration by parts formula for surfaces holds [22]: let $\boldsymbol{\psi} : \Gamma \to \mathbb{R}^d$ be a differentiable function; then,

$$\int_\Gamma \operatorname{div}_\Gamma \boldsymbol{\psi} = \int_\Gamma H\boldsymbol{\nu} \cdot \boldsymbol{\psi} + \int_{\partial\Gamma} \boldsymbol{\psi} \cdot \mathbf{b}, \tag{7}$$

where $\mathbf{b}$ is the unit vector directed tangentially to Γ and normally to $\partial\Gamma$ (cf. Fig. 1).

Since we deal with moving domains, we also recall the Reynolds transport theorem for bulk and boundary integrals:

Proposition 1 (Reynolds transport theorem)**.** *Let Γ be a part of the boundary of a domain Ω, and consider two functionals*

$$J_1(\Omega) = \int_\Omega \varphi, \qquad J_2(\Gamma) = \int_\Gamma \psi,$$

where $\varphi : \Omega \to \mathbb{R}$ and $\psi : \Gamma \to \mathbb{R}$ are generic differentiable functions. If the domain Ω moves with velocity $\mathbf{V}$, the time derivatives of the functionals read as follows:

$$\frac{d}{dt} J_1(\Omega) = \int_\Omega [\partial_t \varphi + \operatorname{div}(\varphi \mathbf{V})], \tag{8a}$$

$$\frac{d}{dt} J_2(\Gamma) = \int_\Gamma [\partial_t \psi + \operatorname{div}_\Gamma(\psi \mathbf{V})]. \tag{8b}$$

Remark 2 (Two dimensional case). For $d = 2$, the contact line $\partial\Gamma$ is actually the union of two points, and $\mathbf{b}$ is the tangential direction prolonging the free surface Γ. The vector $\mathbf{b}_s$ is aligned to the wall Σ (thus simply vertical, in our case), and there is no need to define $\boldsymbol{\tau}_{\partial\Gamma}$.

3. Derivation of the differential problem from variational principles

The present section is devoted to the derivation of the system of equations (3) from physical variational principles. To ease the presentation, we split the derivation into two steps: at first (Sec. 3.1), we will consider Σ_b as an impervious wall (see Fig. 1), and subsequently (Sec. 3.2), mass exchange will be allowed through this boundary. It is worth remarking that the result in Sec. 3.1 has an autonomous interest, e.g. in case droplets on a substrate or sloshing fluid in a tank are regarded [23, 15],

3.1. Step 1: derivation in the case without mass exchange

The kinematic conditions require the motion of the free surface Γ^t to be prescribed by the Eulerian velocity $\mathbf{u}$ (cf. (2)). Moreover, Σ_b is a closed boundary, for this first step, thus we do not make any distinction between the fluid velocity and the domain velocity, namely we consider $\mathbf{V} = \mathbf{u}$. Therefore, the kinematic constraints directly apply on $\mathbf{u}$, that is, for any time t,

$$\mathbf{u} \in \mathcal{U}_{ad} = \left\{ \mathbf{u} : \Omega^t \to \mathbb{R}^d \mid \mathbf{u} \cdot \boldsymbol{\nu} = 0 \text{ on } \Sigma^t,\ \mathbf{u} = \mathbf{0} \text{ on } \Sigma_b,\ \int_{\Omega^t} [(\partial_t \rho + \operatorname{div}(\rho \mathbf{u})] = 0 \right\},$$

where $\rho : \Omega^t \to \mathbb{R}$ is the mass density function. In the definition of the set of admissible velocities we included also the conservation of mass, which can be rephrased locally as

$$\dot{\rho} + \rho \operatorname{div} \mathbf{u} = 0 \qquad \text{in } \Omega^t, \tag{9}$$

with the usual notation $\dot{\rho} = \partial_t \rho + \mathbf{u} \cdot \nabla \rho$ for the Lagrangian derivative.

Regarding dynamics, we assume that only gravity and surface tension act on the system. Being such forces conservative, the system possesses a potential energy

$$\mathcal{V} = -\int_{\Omega^t} \rho \mathbf{g} \cdot \mathbf{x} + \int_{\Gamma^t} \gamma + \int_{\Sigma^t} \gamma_l + \int_{\Sigma_g^t} \gamma_g, \tag{10}$$

where the last three terms take into account the pairwise interactions between the fluid in Ω^t, the gas above and the solid wall. In the following, we denote by $|\cdot|$ the measure of a set. Combining Prop. 1 with (4),(7) and (9), and since γ and $\mathbf{g}$ are constant and Σ^t and Σ_g^t are flat, the active power that the environment transfers to the system can be written as

$$\begin{aligned}
\mathcal{W}_a = -\dot{\mathcal{V}} &= \int_{\Omega^t} \rho \mathbf{g} \cdot \mathbf{u} + \gamma \frac{d}{dt} |\Gamma^t| + (\gamma_l - \gamma_g) \frac{d}{dt} |\Sigma^t| \\
&= \int_{\Omega^t} \rho \mathbf{g} \cdot \mathbf{u} - \int_{\Gamma^t} \gamma H \boldsymbol{\nu} \cdot \mathbf{u} - \int_{\partial \Gamma^t} [\gamma \mathbf{u} \cdot \mathbf{b} + (\gamma_l - \gamma_g) \mathbf{u} \cdot \mathbf{b}_s] \\
&= \int_{\Omega^t} \rho \mathbf{g} \cdot \mathbf{u} - \int_{\Gamma^t} \gamma H \boldsymbol{\nu} \cdot \mathbf{u} - \int_{\partial \Gamma^t} \gamma (\cos\theta - \cos\theta_s) \mathbf{u} \cdot \mathbf{b}_s,
\end{aligned}$$

where in the last line we employed the decomposition $\mathbf{u} = (\mathbf{u} \cdot \boldsymbol{\nu}|_{\Sigma^t}) \boldsymbol{\nu}|_{\Sigma^t} + (\mathbf{u} \cdot \boldsymbol{\tau}_{\partial\Gamma}) \boldsymbol{\tau}_{\partial\Gamma} + (\mathbf{u} \cdot \mathbf{b}_s) \mathbf{b}_s$ on $\partial\Gamma^t$ and the identities $\mathbf{u} \cdot \boldsymbol{\nu}|_{\Sigma^t} = \boldsymbol{\tau}_{\partial\Gamma} \cdot \mathbf{b}_s = 0$ and $\mathbf{b} \cdot \mathbf{b}_s = \cos\theta$.

The power transfer $\mathcal{W}_a$ affects different forms of energy of the system. A part of it determines an increase in the kinetic energy $\mathcal{K}$ of the fluid

$$\mathcal{K} = \frac{1}{2} \int_{\Omega^t} \rho |\mathbf{u}|^2,$$

another part is stored as free energy $\mathcal{F}$ with mass-specific density $\psi = \psi(\rho)$, just depending on ρ [20],

$$\mathcal{F} = \int_{\Omega^t} \rho \psi,$$

and, since the fluid is not perfect, a part of this energy is dissipated, resulting in a entropy production $\dot{\mathcal{S}}$. The connection between the quantities defined above is given by the First Law of Thermodynamics that, in the case of adiabatic, isothermal transformations, reads

$$T\dot{\mathcal{S}} = \mathcal{W}_a - \dot{\mathcal{K}} - \dot{\mathcal{F}}. \tag{11}$$

In this identity, the left-hand side $\mathcal{D} = T\dot{\mathcal{S}}$ is called the *total dissipation* function, whereas the right-hand side $\mathcal{W} = \mathcal{W}_a - \dot{\mathcal{K}} - \dot{\mathcal{F}}$ (called *total power* in [20]) represents the amount of power that the system receives and does not transform in kinetic or free energy. From the Second Law of Thermodynamics, we know that

it has to hold $\mathcal{D} \geq 0$, but in order to give this dissipation an explicit expression, we need to introduce a suitable constitutive relation. For the system described in Sec. 2, it is quite natural to assume that the only sources of dissipation are friction on the wall Σ^t and viscosity inside the fluid, thus we can give a consitituive relation for $\mathcal{D}$ in terms of the following Rayleigh dissipation function:

$$\mathcal{R} = \frac{1}{2}\int_{\Omega^t} \mu |D(\mathbf{u})|^2 + \frac{1}{2}\int_{\Sigma^t} \widetilde{\beta} |\Pi_\Sigma \mathbf{u}|^2,$$

by setting $\mathcal{D} = 2\mathcal{R}$.

Now, in order to write the First Law (11), we need an explicit expression of the total power $\mathcal{W}$. In particular, we are going to show that it has the following form:

$$\mathcal{W} = \int_{\Omega^t} \mathbf{B} \cdot \mathbf{u} + \int_{\partial\Omega^t \setminus \Sigma_b} \mathbf{T} \cdot \mathbf{u}, \tag{12}$$

where $\mathbf{B} : \Omega^t \to \mathbb{R}^d$ and $\mathbf{T} : \partial\Omega^t \setminus \Sigma_b \to \mathbb{R}^d$ are suitably defined generalized forces. The expressions for these two quantities can be retrieved by computing the time derivatives of the kinetic and free energies, and employing the definition of $\mathcal{W}$. Indeed, using the equation of conservation of mass (9) and Reynolds transport theorem (8a), one can find that

$$\dot{\mathcal{K}} = \int_{\Omega^t} \rho \mathbf{u} \cdot \dot{\mathbf{u}}, \qquad \dot{\mathcal{F}} = \int_{\Omega^t} \rho \dot{\psi} = \int_{\Omega^t} \rho \psi' \dot{\rho} = -\int_{\Omega^t} \rho^2 \psi' \mathrm{div}\, \mathbf{u}.$$

Concerning the free energy, it is commonly accepted (see, e.g., [20]) that pressure is related to the derivative of the free energy density as

$$\widetilde{p} = \rho^2 \psi'.$$

Thence, after integration by parts of the pressure term, the expression (12) of the total power $\mathcal{W}$ can be written in terms of the generalized forces

$$\mathbf{B} = \rho \mathbf{g} - \rho \dot{\mathbf{u}} - \nabla \widetilde{p}, \qquad \mathbf{T} = \begin{cases} (\widetilde{p} - \gamma H)\boldsymbol{\nu} & \text{on } \Gamma^t, \\ \widetilde{p}\boldsymbol{\nu} & \text{on } \Sigma^t, \\ -\gamma(\cos\theta - \cos\theta_s)\mathbf{b}_s & \text{on } \partial\Gamma^t. \end{cases}$$

At this point, we have all the ingredients to formulate a variational principle from which to derive the equations of the motion for our physical system:

Principle of minimum constrained dissipation. [20, p.119] [3] *For a deformable body undergoing a process with total power $\mathcal{W}$ and Rayleigh dissipation function $\mathcal{R}$, that obeys the Second Law of Thermodynamics in the form $\mathcal{D} \geq 0$, with $\mathcal{D} = 2\mathcal{R}$, the true evolution $\mathbf{u}$ at time t is such that $\mathcal{R}$ attains its minimum w.r.t. all virtual process rates $\widehat{\mathbf{u}} = \mathbf{u} + \delta\mathbf{u}$, once $\mathcal{W}$ and the generalized forces $\mathbf{B}, \mathbf{T}$ are held fixed.*

From the formulation of this principle, we see that one should take into account the constraint of holding both $\mathcal{W}$ and the generalized forces fixed, while varying the velocity field by a term $\delta\mathbf{u}$. In order to do this, it is useful to rewrite the principle in terms of a *reduced* dissipation functional. Following the ideas in [20], we can introduce the Lagrangian functional

$$\mathcal{L} = \mathcal{R} + \lambda \mathcal{W},$$

where λ is the Lagrange multiplier for the imposition of the constraint over $\mathcal{W}$, during the minimization of $\mathcal{R}$. Aiming at enforcing the variations of $\mathcal{L}$ to be equal to zero, we compute the variations of $\mathcal{R}$ and $\mathcal{W}$

[3] In the present work, we are adopting the viewpoint of Continuum Mechanics, thus we talk about *minimum* dissipation. In the literature of Statistical Mechanics, this principle is looked at as a *maximum* principle. However, for the purposes of the present work, only the stationarity of the functional is considered, hence we avoid digging any further into this distinction.

induced by a virtual velocity variation $\delta\mathbf{u}$. Concerning the Rayleigh dissipation functional, it is enough to compute the Gâteaux derivative

$$\delta\mathcal{R} = \partial_{\mathbf{u}}\mathcal{R}[\delta\mathbf{u}] = \int_{\Omega^t} 2\mu D(\mathbf{u}) \cdot D(\delta\mathbf{u}) + \int_{\Sigma^t} \widetilde{\beta}\, \Pi_\Sigma \mathbf{u} \cdot \Pi_\Sigma \delta\mathbf{u}.$$

Dealing with the total power, the Principle requires to hold $\mathbf{B}$ and $\mathbf{T}$ fixed. Therefore, instead of using the classical Gâteaux derivative, we define the variation of $\mathcal{W}$ as

$$\delta\mathcal{W} = \int_{\Omega^t} \mathbf{B} \cdot \delta\mathbf{u} + \int_{\partial\Omega^t \setminus \Sigma_b} \mathbf{T} \cdot \delta\mathbf{u}.$$

Now we can compute the variations of the Lagrangian functional $\mathcal{L}$ induced by $\delta\mathbf{u}$:

$$0 = \delta\mathcal{L} = \delta\mathcal{R} + \lambda\delta\mathcal{W} = (\partial_{\mathbf{u}}\mathcal{R} + \lambda\delta_{\mathbf{u}}\mathcal{W})\,[\delta\mathbf{u}], \qquad \forall\delta\mathbf{u},$$

where we have introduced the linear functional $\delta_{\mathbf{u}}\mathcal{W} : \delta\mathbf{u} \mapsto \delta\mathcal{W}$, with $\delta\mathcal{W}$ defined as above. Now, the value of the Lagrange multiplier λ can be found by imposing the validity of the First Law of Thermodynamics (11), which can be rewritten as

$$2\mathcal{R} = \mathcal{D} = \mathcal{W}. \tag{13}$$

Indeed, since $\partial_{\mathbf{u}}\mathcal{R}[\mathbf{u}] = 2\mathcal{R}$ and $\delta_{\mathbf{u}}\mathcal{W}[\mathbf{u}] = \mathcal{W}$, combining (13) with $(\partial_{\mathbf{u}}\mathcal{R} + \lambda\delta_{\mathbf{u}}\mathcal{W})[\mathbf{u}] = 0$ yields $\lambda = -1$. Therefore, the principle of minimum constrained dissipation can be equivalently formulated as follows:

Principle of minimum reduced dissipation. [20, p.137] *For a deformable body undergoing a process with total power $\mathcal{W}$ and Rayleigh dissipation function $\mathcal{R}$, that obeys the Second Law of Thermodynamics in the form $\mathcal{D} \geq 0$, with $\mathcal{D} = 2\mathcal{R}$, the true evolution $\mathbf{u}$ at time t is such that the reduced dissipation function $\widetilde{\mathcal{R}} = \mathcal{R} - \mathcal{W}$ attains its minimum w.r.t. all virtual process rates $\widehat{\mathbf{u}} = \mathbf{u} + \delta\mathbf{u}$, once the generalized forces $\mathbf{B}, \mathbf{T}$ are held fixed. That is, the true evolution is characterized by the requirement that*

$$\delta\mathcal{R} = \delta\mathcal{W} \qquad \text{in any subregion } \omega \subseteq \Omega^t, \tag{14}$$

where $\delta\mathcal{R} = \partial_{\mathbf{u}}\mathcal{R}[\delta\mathbf{u}]$, $\delta\mathcal{W} = \int_{\Omega^t} \mathbf{B} \cdot \delta\mathbf{u} + \int_{\Gamma^t} \mathbf{T} \cdot \delta\mathbf{u}$.

Now we can apply this principle in our settings, in order to obtain the differential equations governing the physical phenomenon at hand. We also assume that the fluid in Ω^t is incompressible, hence we can divide both sides of (14) by the constant density ρ, without losing generality. [4] Thus, rephrasing the optimality condition (14) and writing explicitly the total derivative $\frac{d}{dt}\mathbf{u} = \partial_t\mathbf{u} + \mathbf{u} \cdot \nabla\mathbf{u}$ yield

$$\begin{aligned}\int_\omega 2\nu D(\mathbf{u}) \cdot D(\delta\mathbf{u}) + \int_{\partial\omega\cap\Sigma^t} \beta\, \Pi_\Sigma\mathbf{u} \cdot \Pi_\Sigma\delta\mathbf{u} \\ = -\int_\omega [(\partial_t\mathbf{u} + \mathbf{u}\cdot\nabla\mathbf{u} - \mathbf{g}) \cdot \delta\mathbf{u} - p\,\mathrm{div}\,\delta\mathbf{u}] - \int_{\partial\omega\cap\Gamma^t} \gamma H \delta\mathbf{u}\cdot\boldsymbol{\nu} - \int_{\partial\omega\cap\partial\Gamma^t} \gamma(\cos\theta - \cos\theta_s)\delta\mathbf{u}\cdot\mathbf{b}_s,\end{aligned}$$

where $\beta = \widetilde{\beta}/\rho$. Integrating by parts and using the kinematic conditions $\mathbf{u}\cdot\boldsymbol{\nu} = 0$ on Σ^t, $\delta\mathbf{u} = 0$ on Σ_b, we obtain

$$\begin{aligned}\int_\omega (\partial_t\mathbf{u} + \mathbf{u}\cdot\nabla\mathbf{u} - \mathrm{div}\,(2\nu D(\mathbf{u})) + \nabla p - \mathbf{g}) \cdot \delta\mathbf{u} + \int_{\partial\omega\cap\Gamma^t} (\gamma H\boldsymbol{\nu} + 2\nu D(\mathbf{u})\boldsymbol{\nu} - p\boldsymbol{\nu}) \cdot \delta\mathbf{u} \\ + \int_{\partial\omega\cap\partial\Gamma^t} \gamma(\cos\theta - \cos\theta_s)\delta\mathbf{u}\cdot\mathbf{b}_s + \int_{\partial\omega\cap\Sigma^t} \Pi_\Sigma\,(\beta\mathbf{u} - 2\nu D(\mathbf{u})\boldsymbol{\nu} + p\boldsymbol{\nu}) \cdot \Pi_\Sigma\delta\mathbf{u} = 0.\end{aligned} \tag{15}$$

[4] Keeping the density ρ explicit until the very end helped in keeping the presentation general and relatively simple. If we had imposed the uniformity of ρ since the beginning, no free energy $\mathcal{F}$ would have appeared, and the rescaled pressure p would have needed to be introduced as a Lagrange multiplier for the incompressibility constraint, rather complicating the argument.

Since $\delta\mathbf{u}$ is arbitrary, as well as the subregion ω, from (15) we can derive the strong formulation of the Navier-Stokes equations with moving contact line. Such equations, combined with the kinematic condition $\mathbf{V}\cdot\boldsymbol{\nu} = \mathbf{u}\cdot\boldsymbol{\nu}$ on $\partial\Omega^t$ (see Remark 1) and the constraint $\mathbf{V}\cdot\boldsymbol{\nu} = 0$ on Σ^t (see $\mathcal{U}_{ad}$ in Sec. 2), make up the following differential problem:

$$\begin{cases} \partial_t\mathbf{u} + (\mathbf{u}\cdot\nabla)\mathbf{u} - \operatorname{div}\sigma = \mathbf{g} & \text{in } \Omega^t, \\ \operatorname{div}\mathbf{u} = 0 & \text{in } \Omega^t, \\ \mathbf{V}\cdot\boldsymbol{\nu} = \mathbf{u}\cdot\boldsymbol{\nu} & \text{on } \Gamma^t \\ \sigma\boldsymbol{\nu}\cdot\boldsymbol{\tau} = 0, \quad \sigma\boldsymbol{\nu}\cdot\boldsymbol{\nu} + \gamma H = 0 & \text{on } \Gamma^t, \forall\boldsymbol{\tau}\perp\boldsymbol{\nu}, \\ \mathbf{u}\cdot\boldsymbol{\nu} = 0, \quad (\sigma\boldsymbol{\nu} + \beta\mathbf{u} + \gamma(\cos\theta - \cos\theta_s)\delta_{\partial\Gamma}\,\mathbf{b}_s)\cdot\boldsymbol{\tau} = 0 & \text{on } \Sigma^t, \forall\boldsymbol{\tau}\perp\boldsymbol{\nu}, \end{cases}$$

where $\sigma = 2\nu D(\mathbf{u}) - pI$ is the stress tensor. This problem is well defined for the whole time evolution as soon as we know the initial condition $\mathbf{u}(t=0) = \mathbf{u}^0$.

Before passing to the second step of our derivation, we point out that, in the incompressible case, the introduction of the free energy $\mathcal{F}$ occurs to be just instrumental to take into account the pressure p in the equations (this will be true also in the next section). This is the reason why we will not introduce a discrete free energy, in Sec. 5.

3.2. Step 2: allowing mass exchanges with the environment

So far, we have considered a closed physical system, in terms of mass exchange. However, taking into account the possibility of having an inflow/outflow boundary is a necessity when modeling many phenomena. In this section, we allow the fluid to pass through the boundary Σ_b (see Fig. 1). This part of the domain boundary is going to be fixed in the domain evolution, but in order to flow through it, the fluid may have a nonzero normal velocity $\mathbf{u}\cdot\boldsymbol{\nu}$ at Σ_b. Moreover, we account for a possible external surface load $\boldsymbol{\zeta}$, acting on the open boundary.

In these new settings, we need to perform some modifications on the definition of the energetic quantities managed above, and on their relationships. First of all, since our domain is not moving in a Lagrangian way together with the particles it contains, the time variation of the physical quantities are not given anymore by their Lagrangian derivative along the fluid velocity $\mathbf{u}$. Therefore, we introduce a different notation for the total derivative along the domain velocity field $\mathbf{V}$: for a scalar field like density we write

$$D_t\rho = \partial_t\rho + \mathbf{V}\cdot\nabla\rho.$$

A similar notation is going to be used for integral quantities, like the free energy: the application of Prop. 1 yields

$$D_t\mathcal{F} = \int_{\Omega^t} \left[\partial_t(\rho\psi) + \operatorname{div}(\rho\psi\mathbf{V})\right].$$

According to this definition for the time derivative, the active power $\mathcal{W}_a$, including also the contribution due to the external surface stress, is now of the form

$$\mathcal{W}_a = -D_t\mathcal{V} + \int_{\Omega^t} \boldsymbol{\zeta}\cdot\mathbf{u}.$$

Eventually, the total power has to include also the energy flux associated with the mass flowing through the open boundary Σ_b, whence it has to be re-defined as

$$\mathcal{W} = -D_t\mathcal{V} - D_t\mathcal{K} - D_t\mathcal{F} + \int_{\Omega^t}\boldsymbol{\zeta}\cdot\mathbf{u} - \int_{\Sigma_b}\left(\frac{1}{2}\rho|\mathbf{u}|^2 - \mathbf{g}\cdot\mathbf{x} + \rho\psi\right)\mathbf{u}\cdot\boldsymbol{\nu}. \tag{16}$$

Having these new definitions, we can perform all the steps followed in Sec. 3.1, up to formally writing the principle of minimum reduced dissipation (14). The last ingredient we need, in order to obtain the differential equation ruling the physical phenomenon at hand, is the definition of the generalized forces

$\mathbf{B}, \mathbf{T}$. To this aim, we need to write explicitly all the quantities appearing in (16). For the sake of brevity, let us compute explicitly only the total time derivative of the kinetic energy:

$$D_t\mathcal{K} = \int_{\Omega^t} \left[\frac{1}{2}|\mathbf{u}|^2 \left(\partial_t\rho + \mathbf{V}\cdot\nabla\rho + \rho \mathrm{div}\,\mathbf{V}\right) + \rho\mathbf{u}\cdot\partial_t\rho + \frac{1}{2}\rho\mathbf{V}\cdot\nabla|\mathbf{u}|^2 \right].$$

Noticing that if $\mathbf{V} = \mathbf{u}$ we would have the Lagrangian time derivative $\dot{\mathcal{K}}$, we can write the expression above in terms of $\dot{\mathcal{K}}$ itself, as follows:

$$\begin{aligned} D_t\mathcal{K} &= \dot{\mathcal{K}} + \int_{\Omega^t} \left[\frac{1}{2}|\mathbf{u}|^2(\mathbf{V}-\mathbf{u})\cdot\nabla\rho + \frac{1}{2}\rho(\mathbf{V}-\mathbf{u})\cdot\nabla|\mathbf{u}|^2 + \frac{1}{2}\rho|\mathbf{u}|^2 \mathrm{div}\,(\mathbf{V}-\mathbf{u}) \right] \\ &= \dot{\mathcal{K}} + \int_{\Omega^t} \mathrm{div}\, \left[\frac{1}{2}\rho|\mathbf{u}|^2(\mathbf{V}-\mathbf{u}) \right] = \dot{\mathcal{K}} + \int_{\Sigma_b} \frac{1}{2}\rho|\mathbf{u}|^2(\mathbf{V}-\mathbf{u})\cdot\boldsymbol{\nu} \\ &= \dot{\mathcal{K}} - \int_{\Sigma_b} \frac{1}{2}\rho|\mathbf{u}|^2\mathbf{u}\cdot\boldsymbol{\nu}, \end{aligned}$$

where we have used that $\mathbf{V}\cdot\boldsymbol{\nu} = \mathbf{u}\cdot\boldsymbol{\nu}$ on $\Gamma^t \cup \Sigma^t$. As we can see, the difference between the total derivative of the kinetic energy contained in Ω^t and its Lagrangian derivative is given by the opposite of the exiting flux through Σ_b. Analogous computations for the potential energy and the free energy lead to similar results, thence the total power can be written also as

$$\mathcal{W} = -\dot{\mathcal{V}} - \dot{\mathcal{K}} - \dot{\mathcal{F}} + \int_{\Omega^t} \boldsymbol{\zeta}\cdot\mathbf{u},$$

where the flux terms have been canceled out in the transition from D_t to the derivative $\dot{(\cdot)}$. Therefore, the generalized forces $\mathbf{B}, \mathbf{T}$ read as follows:

$$\mathbf{B} = \rho\mathbf{g} - \rho\dot{\mathbf{u}} - \nabla\widetilde{p}, \qquad \mathbf{T} = \begin{cases} (\widetilde{p} - \gamma H)\boldsymbol{\nu} & \text{on } \Gamma^t, \\ \widetilde{p}\boldsymbol{\nu} & \text{on } \Sigma^t, \\ \widetilde{p}\boldsymbol{\nu} + \boldsymbol{\zeta} & \text{on } \Sigma_b, \\ -\gamma(\cos\theta - \cos\theta_s)\mathbf{b}_s & \text{on } \partial\Gamma^t. \end{cases}$$

Using these expressions, and assuming incompressibility and a homogeneous fluid density, we can employ the Principle of minimum reduced dissipation and eventually obtain system (3).

Remark 3. For the sake of clarity we remark that, although the final steps of the derivation formally employ the Lagrangian derivatives of the energies along $\mathbf{u}$, a physically consistent formulation of the First Law of Thermodynamics for the domain Ω^t considered here can be written only in terms of the material derivatives along $\mathbf{V}$: this is why the correct definition of the total power is actually (16).

Remark 4. In the applied mathematical literature, a variational principle named after Onsager has recently gained some popularity, in the derivation of differential problems [8, 5, 19, 6]. The formulation of this principle is quite similar to identity (14), but its justification is ascribed to Onsager-Casimir reciprocal relations [24, 25], a principle holding at the microscopic level, whereas the Principle of minimum reduced dissipation is purely macroscopic. As pointed out in [20, from p.149], connecting the microscopic reciprocal relations to the macroscopic principle used in the above-mentioned literature is not easy: *"Though no objection could be raised against the reversibility of microscopic motions, its reverberations on a macroscopic scale are invariably the object of an assumption, in one fashion or another"*. Therefore, in the present work we decided to adopt the procedure developed in [20], in the frameworks of Analytic and Continuum Mechanics, avoiding the need of microscopical considerations. This choice gave us a general workflow that could be used to treat both the closed-system case (Sec. 3.1) and the case with mass exchange (Sec. 3.2). In this regard, it is worth pointing out that the latter case was not considered in [20].

4. Discretization of the problem

After the introduction and justification of the system (3), now we address its numerical solution, and thence we introduce its discretization via the Finite Element Method (FEM). As usual, we first reformulate the system in a suitable weak form, taking into account the domain motion. For the first part of this section, the domain velocity $\mathbf{V}$ will be considered as known: the actual coupling of the physical and the geometrical problem will be dealt with in Sec. 4.4.

4.1. Eulerian and ALE weak formulation

The state of the fluid at hand is represented by its static pressure p and its Eulerian velocity $\mathbf{u}$. Due to the presence of the wall Σ^t, the velocity has to comply a kinematic condition, so we introduce the following Hilbert spaces, for the fluid state $(\mathbf{u}, p)$:

$$\begin{aligned}\widetilde{V}^t &= \{\mathbf{v} \in [H^1(\Omega^t)]^d \mid \mathbf{v} \cdot \boldsymbol{\nu} = 0 \text{ on } \Sigma^t\},\\ \widetilde{P}^t &= L^2(\Omega^t).\end{aligned}$$

Testing problem (3) against some $(\mathbf{v}, \pi) \in \widetilde{V}^t \times \widetilde{P}^t$, we can formally write the following weak formulation of the problem: given $\mathbf{u}(t=0) = \mathbf{u}^0$, find $(\mathbf{u}, p)$ such that for all $t > 0$

$$\begin{aligned}(\partial_t \mathbf{u}, \mathbf{v}) + a(\mathbf{u}, \mathbf{v}) + b(\mathbf{v}, p) + c(\mathbf{u}, \mathbf{u}, \mathbf{v}) = F(\mathbf{v}) \quad &\forall \mathbf{v} \in \widetilde{V}^t,\\ b(\mathbf{u}, \pi) = 0 \qquad &\forall \pi \in \widetilde{P}^t,\end{aligned} \tag{17}$$

where

$$\begin{aligned}(\cdot,\cdot) \quad &\text{is the } L^2 \text{ inner product on } \Omega^t,\\ a(\mathbf{u}, \mathbf{v}) &= \Big(\frac{\nu}{2}(\nabla \mathbf{u} + \nabla \mathbf{u}^T), \nabla \mathbf{v} + \nabla \mathbf{v}^T\Big) + \int_{\Sigma^t} \beta \mathbf{u} \cdot \mathbf{v},\\ b(\mathbf{v}, \pi) &= -(\text{div } \mathbf{v}, \pi),\\ c(\mathbf{w}, \mathbf{u}, \mathbf{v}) &= ((\mathbf{w} \cdot \nabla)\mathbf{u}, \mathbf{v}),\\ F(\mathbf{v}) &= (\mathbf{g}, \mathbf{v}) + \int_{\Sigma_b} \boldsymbol{\zeta} \cdot \mathbf{v} - \int_{\Gamma^t} \gamma \text{div}_{\,\Gamma} \mathbf{v} + \int_{\partial\Gamma^t} \gamma \mathbf{v} \cdot \mathbf{b}_s \cos\theta_s.\end{aligned}$$

Remark 5. The derivation of problem (17) from (3) is quite standard [26, 27]. Anyway, a smart use of (7) and some other geometrical considerations – as done in [15] – prevent the curvature H and the current angle θ from explicitly appearing in the formulation (17). This simplifies the numerical treatment of the equations, since the discrete approximation of angles and curvature is not straightforward (e.g., cf. [28]).

Problem (17) is written in Eulerian coordinates, and at a fixed time t. In a numerical discretization, this would imply either keeping the mesh fixed during the time evolution – at the cost of introducing extra theoretical difficulty to deal with the domain movement – or generating a completely new mesh at each time step – thus bringing in a very high computational cost. A widely used technique to have a computationally rather inexpensive mesh motion is to set the equations in an Arbitrary Lagrangian-Eulerian (ALE) framework [13, 14], in which the domain velocity $\mathbf{V}$, defined in (1) is considered separately from the fluid velocity $\mathbf{u}$. Associated to the domain velocity, we can define the so called *ALE derivative operator*, which computes the time derivative of a function $\varphi : \Omega^t \to \mathbb{R}$ along the domain trajectory described by $\mathbf{V}$:

$$\partial_t^{ALE} \varphi = \partial_t \varphi + \mathbf{V} \cdot \nabla \varphi.$$

It is worth pointing out that the domain velocity $\mathbf{V}$ occurs to be the ALE derivative of the position, i.e. $\mathbf{V} = \partial_t^{ALE} \mathbf{x}$. Employing the definition of ∂_t^{ALE}, problem (17) can be formulated in the ALE framework as follows [13, 15]:

$$\begin{aligned}(\partial_t^{ALE} \mathbf{u}, \mathbf{v}) + a(\mathbf{u}, \mathbf{v}) + b(\mathbf{v}, p) + c_{ALE}(\mathbf{u}, \mathbf{V}, \mathbf{u}, \mathbf{v}) = F(\mathbf{v}) \quad &\forall \mathbf{v} \in V^t,\\ b(\mathbf{u}, \pi) = 0 \qquad &\forall \pi \in P^t,\\ \mathbf{u}(t=0) = \mathbf{u}^0,&\end{aligned} \tag{18}$$

where

$$V^t = \{\mathbf{v} : \Omega^t \to \mathbb{R}^d \mid \exists \widehat{\mathbf{v}} \in \widetilde{V}^0, \mathbf{v}(\mathbf{x}) = \widehat{\mathbf{v}}(\mathcal{A}_t^{-1}(\mathbf{x}))\},$$
$$P^t = \{\pi : \Omega^t \to \mathbb{R} \mid \exists \widehat{\pi} \in \widetilde{P}^0, \pi(\mathbf{x}) = \widehat{\pi}(\mathcal{A}_t^{-1}(\mathbf{x}))\},$$
$$c_{ALE}(\mathbf{z}, \mathbf{V}, \mathbf{u}, \mathbf{v}) = \int_{\Omega^t} [(\mathbf{z} - \mathbf{V}) \cdot \nabla] \mathbf{u} \cdot \mathbf{v} - \int_{\Omega^t} \operatorname{div}(\mathbf{V}) \mathbf{u} \cdot \mathbf{v}.$$

4.2. Time discretization

In this section, we discretize the ALE formulation (18) w.r.t. time, using a uniform time discretization made of time steps $t^{(n)} = n\Delta t, n = 0, 1, \ldots, N = \frac{T}{\Delta t}$. Such a semi-discretization also involves the domain motion, thus we need to discretize the ALE map, introducing the application

$$\mathcal{A}_{n,n+1} : \Omega^{(n)} \to \Omega^{(n+1)}, \qquad \mathcal{A}_{n,n+1}(\mathbf{x}) = \mathbf{x} + \Delta t \, \mathbf{V}^{(n)}(\mathbf{x}),$$

where the superscript (n) indicates the time step $t^{(n)}$ at which the quantity is taken (e.g. $\mathbf{V}^{(n)}(\mathbf{x}) = \mathbf{V}(t^{(n)}, \mathbf{x})$): this notation will be used for all the other quantities involved in the problem. The discretization of the ALE map directly induces the definition of a discrete sequence of domains $\Omega^{(n)} = \mathcal{A}_{n-1,n}(\Omega^{(n-1)})$, on which the following spaces are recursively defined as

$$\begin{aligned} V^{(n)} &= \{\mathbf{v} \in [H^1(\Omega^{(n)})]^d \mid \mathbf{v} \circ \mathcal{A}_{n-1,n} \in V^{(n-1)}\}, \\ P^{(n)} &= \{p \mid p \circ \mathcal{A}_{n-1,n} \in P^{(n-1)}\}, \end{aligned} \tag{19}$$

where $V^{(0)}, P^{(0)}$ are assigned. Thus one reduces to building up a basis only for the initial spaces $V^{(0)}$ and $P^{(0)}$, the bases for $V^{(n)}$ and $P^{(n)}$ being obtained via the maps $\mathcal{A}_{i-1,i}, i = 1, \ldots, n$. This represents a remarkable computational saving in the numerical solution of the problem. It is worth noticing that having each $\mathbf{V}^{(n)}$ to belong to $\mathcal{U}_{ad}$, the kinematic constraints are preserved, and at each time $t^{(n)}$ the spaces actually correspond to the usual definition, i.e.

$$\begin{aligned} V^{(n)} &= \{\mathbf{v} \in [H^1(\Omega^{(n)})]^d \mid \mathbf{v} \cdot \boldsymbol{\nu} = 0 \text{ on } \Sigma^{(n)}\}, \\ P^{(n)} &= L^2(\Omega^{(n)}). \end{aligned}$$

In view of the above discussion, the time-discretization of problem (3) reads as follows: given $\mathbf{u}^{(0)}$, for each $n = 0, \ldots, N-1$, find $(\mathbf{u}^{(n+1)}, p^{(n+1)}) \in V^{(n+1)} \times P^{(n+1)}$ such that, $\forall (\mathbf{v}, \pi) \in V^{(n)} \times P^{(n)}$,

$$\begin{aligned} &\frac{1}{\Delta t}(\mathbf{u}^{(n+1)}, \mathbf{v})_{\Omega^{(n+1)}} + a^{(n+1)}(\mathbf{u}^{(n+1)}, \mathbf{v}) + b^{(n+1)}(\mathbf{v}, p^{(n+1)}) \\ &+ c_{ALE}^{(n+1)}(\mathbf{u}^{(n)}, \mathbf{V}^{(n)}, \mathbf{u}^{(n+1)}, \mathbf{v}) + s^{(n+1)}(\mathbf{V}^{(n)}, \mathbf{u}^{(n)}, \mathbf{u}^{(n+1)}, \mathbf{v}) = \frac{1}{\Delta t}(\mathbf{u}^{(n)}, \mathbf{v})_{\Omega^{(n)}} + F^{(n+1)}(\mathbf{v}), \\ &\qquad\qquad b^{(n+1)}(\mathbf{u}^{(n+1)}, \pi) = 0, \end{aligned} \tag{20}$$

where the superscript (n) in the spaces and forms indicates that the domain under consideration is $\Omega^{(n)}$. The additional form $s^{(n+1)}(\cdot, \cdot, \cdot)$ artificially adds the following strongly consistent stabilization terms:

$$s^{(n+1)}(\mathbf{V}^{(n)}, \mathbf{u}^{(n)}, \mathbf{u}^{(n+1)}, \mathbf{v}) = \frac{1}{2} \int_{\Omega^{(n+1)}} \operatorname{div}(\mathbf{u}^{(n)}) \mathbf{u}^{(n+1)} \cdot \mathbf{v} - \frac{1}{2} \int_{\Gamma^{(n+1)}} (\mathbf{u}^{(n)} - \mathbf{V}^{(n)}) \cdot \boldsymbol{\nu} \, \mathbf{u}^{(n+1)} \cdot \mathbf{v},$$

whose presence is widely accepted in the ALE literature [29, 27] and whose role will be clear from the proof of Thm. 1, in Sec. 5.

Remark 6. In the terms involved in (20), the domain of integration does not always coincide with the domain of definition of the integrands, e.g. $\mathbf{v}$ is defined on $\Omega^{(n)}$, but it appears in integrals over $\Omega^{(n+1)} = \mathcal{A}_{n,n+1}(\Omega^{(n)})$. In order to keep a light notation, a change of variables via ALE mapping is understood in case this discordance occurs: e.g. $\int_{\Omega^{(n+1)}} \mathbf{v}$ actually means $\int_{\Omega^{(n+1)}} \mathbf{v} \circ \mathcal{A}_{n,n+1}^{-1}$.

4.3. The fully discrete problem

In this section, we introduce the space discretization for the problem under inspection. To this aim, let $\mathcal{T}_h^{(0)}$ be a regular triangulation [30] of the initial domain $\Omega^{(0)}$, with characteristic discretization step h. The triangulation of $\Omega^{(n)}$ is obtained through repeated applications of the discrete ALE map, i.e. $\mathcal{T}_h^{(n)} = \mathcal{A}_{n-1,n}\left(\mathcal{T}_h^{(n-1)}\right)$. In these settings, we can write the FEM approximation of problem (20) as follows: given the FEM interpolation $\mathbf{u}_h^{(0)}$ of the initial velocity field $\mathbf{u}^{(0)}$, for each $n = 0, \dots, N-1$, find $(\mathbf{u}_h^{(n+1)}, p_h^{(n+1)}) \in V_h^{(n+1)} \times P_h^{(n+1)}$ such that, $\forall (\mathbf{v}_h, \pi_h) \in V_h^{(n)} \times P_h^{(n)}$,

$$\begin{aligned}\frac{1}{\Delta t}(\mathbf{u}_h^{(n+1)}, \mathbf{v}_h)_{\Omega^{(n+1)}} + a^{(n+1)}(\mathbf{u}_h^{(n+1)}, \mathbf{v}_h) + b^{(n+1)}(\mathbf{v}_h, p_h^{(n+1)}) - b^{(n+1)}(\mathbf{u}_h^{(n+1)}, \pi_h) \\ + c_{ALE}^{(n+1)}(\mathbf{u}_h^{(n)}, \mathbf{V}_h^{(n)}, \mathbf{u}_h^{(n+1)}, \mathbf{v}_h) + s^{(n+1)}(\mathbf{V}_h^{(n)}, \mathbf{u}_h^{(n)}, \mathbf{u}_h^{(n+1)}, \mathbf{v}_h) \\ = \frac{1}{\Delta t}(\mathbf{u}_h^{(n)}, \mathbf{v}_h)_{\Omega^{(n)}} + F^{(n+1)}(\mathbf{v}_h),\end{aligned} \tag{21}$$

where

$$V_h^{(0)} = V^{(0)} \cap [X_h^{r_\mathbf{u}}(\Omega)]^d, \qquad P_h^{(0)} = P^{(0)} \cap X_h^{r_p}(\Omega),$$
$$X_h^r(\Omega) = \left\{\varphi \in C^0\left(\overline{\Omega}\right) \mid \varphi|_K \in \mathbb{P}_r(K)\ \forall K \in \mathcal{T}_h^{(0)}\right\},$$

and $V_h^{(n)}, P_h^{(n)}$ are recursively defined in the same way as in (19).

Remark 7 (Variational crime). Here we do not make a distinction between the evolution of the domain according to the continuous map $\mathcal{A}_t$ and the sequence of discrete maps $\mathcal{A}_{n-1,n}$. This is related to the well-known (and usually disregarded) variational crime [31].

In the formulation (21), the polynomial degrees $r_\mathbf{u}, r_p$ still need to be chosen. In the present work, we focus on the $\mathbb{P}_1 - \mathbb{P}_1$ pair, namely the case $r_\mathbf{u} = r_p = 1$: a comment on this choice will be made after the introduction of the problem for the domain velocity $\mathbf{V}^{(n)}$, at the end of Sec. 4.4. Hence, in order to cope with the lack of validity of the LBB condition (cf. [32, 27]), we employ the classical Brezzi-Pitkäranta pressure stabilization [33], replacing the form $s^{(n+1)}$ in problem (21) with the form

$$\begin{aligned}s_p^{(n+1)}(\mathbf{V}_h^{(n)}, \mathbf{u}_h^{(n)}, \mathbf{u}_h^{(n+1)}, \mathbf{v}_h, p_h^{(n+1)}, \pi_h) = s^{(n+1)}(\mathbf{V}_h^{(n)}, \mathbf{u}_h^{(n)}, \mathbf{u}_h^{(n+1)}, \mathbf{v}_h) \\ + C_s h^2 \sum_{K \in \mathcal{T}_h^{(n)}} \int_K \nabla p_h^{(n+1)} \cdot \nabla \pi_h.\end{aligned} \tag{22}$$

So far we assumed the knowledge of the domain velocity $\mathbf{V}$. However, this is part of the unknowns and the following section addresses the construction of the (discrete) geometrical velocity $\mathbf{V}^{(n)}$, which allows to pass from $\Omega^{(n)}$ to $\Omega^{(n+1)}$.

4.4. Kinematic conditions

As anticipated in Sec. 2, the domain velocity $\mathbf{V}$ has to undergo some kinematic conditions, in order to ensure a physically consistent evolution of the domain. In particular, being Σ^t a solid wall, and as the motion of the fluid particles follows the free boundary Γ^t, the domain velocity must satisfy

$$\mathbf{V} \cdot \boldsymbol{\nu} = 0 \qquad \text{on } \Sigma^t, \tag{23a}$$
$$\mathbf{V} \cdot \boldsymbol{\nu} = \mathbf{u} \cdot \boldsymbol{\nu} \qquad \text{on } \Gamma^t, \tag{23b}$$

at any time t. Moreover, since Σ_b is held fixed, we also require $\mathbf{V} \cdot \boldsymbol{\nu} = 0$ on Σ_b. In view of the discussion in Remark 1, these conditions are sufficient to determine the overall evolution of the domain Ω^t. Therefore, we require the same conditions for the discrete domain velocity $\mathbf{V}_h^{(n)}$.

We remark that, since $\mathbf{V}_h^{(n)}$ is used to move the mesh, we need an explicit knowledge of all its components at the whole set of mesh nodes. However, conditions like (23) prescribe only one degree of freedom of the boundary distribution of such velocity. Hence, we can fix all the other degrees of freedom by requiring $\mathbf{V}_h^{(n)}$ to be vertical, namely $\mathbf{V}_h^{(n)} = v_h^{(n)}\mathbf{e}_d$. This yields some useful properties, that will be displayed in Prop. 2. Then, to determine the bulk distribution of the velocity, we consider a harmonic lifting, which is a widely adopted choice in the ALE literature [34, 35, 15] since it generates a regular velocity field, whence the mapped mesh preserves a certain degree of regularity.

Summarizing, the domain velocity $\mathbf{V}_h^{(n)}$ mapping $\mathcal{T}_h^{(n)}$ to $\mathcal{T}_h^{(n+1)}$ can be defined as the solution of the following problem: prescribing $\mathbf{V}_h^{(n)}$ to be vertical, namely $\mathbf{V}_h^{(n)} = v_h^{(n)}\,\mathbf{e}_d$, find $v_h^{(n)} \in X_h^1(\Omega^{(n)})$ such that

$$\begin{cases} \Delta v_h^{(n)} = 0 & \text{in } \Omega^{(n)}, \\ v_h^{(n)} = 0 & \text{on } \Sigma_b, \\ \partial_{\boldsymbol{\nu}} v_h^{(n)} = 0 & \text{on } \Sigma^{(n)}, \\ v_h^{(n)}\nu_d = \mathbf{u}_h^* \cdot \boldsymbol{\nu} & \text{on } \Gamma^{(n)}, \end{cases} \tag{24}$$

where $\mathbf{u}_h^* : \Gamma^{(n)} \to \mathbb{R}^d$ is some discrete counterpart of the fluid velocity $\mathbf{u}$. Different definitions can be given for $\mathbf{u}_h^*$, and they have a nonnegligible effect on the stability of the numerical scheme as a whole (cf. Sec. 5). In our numerical tests, we adopt the simplest choice for such a velocity, that is, we set

$$\mathbf{u}_h^* = \mathbf{u}_h^{(n)}, \tag{25}$$

which corresponds to an explicit treatment of the geometry. In the next section we will analyze its impact on the scheme, and propose an original strategy to cure possible instabilities associated to it.

Another possibility, that is also considered in Sec. 5, is the implicit treatment of the geometry, determined by

$$\mathbf{u}_h^* = \mathbf{u}_h^{(n+1)} \circ \mathcal{A}_{n,n+1}. \tag{26}$$

This choice, however, introduces a high nonlinearity in the system, due to the strong coupling between the physical problem (18) and the geometrical problem (24). Thus, some nonlinear solver is required, and the computational effort is much higher than in the explicit case. This may represent a serious obstruction in case the state problem needs to be solved many times for different parameter values (e.g., in optimal control problems).

Other choices for $\mathbf{u}_h^*$ can be straightforwardly introduced in the scheme, like the extrapolation proposed in [15]:

$$\mathbf{u}_h^* = 2\mathbf{u}^{(n)} - \mathbf{u}^{(n-1)} \circ \mathcal{A}_{n-1,n}^{-1},$$

which benefits from the inexpensiveness of the explicit treatment and, in the numerical test cases considered in [15], does not show stability issues. However, up to the authors' knowledge, no theoretical results are known on the stability of the scheme characterized by this extrapolation.

Concluding this section, we comment on some implementation aspects. The choice of piecewise linear elements for the fluid velocity was made in order to ease the implementation, by avoiding curvilinear elements and thus isoparametric finite elements. Eventually, we remark that the actual kinematic condition $v_h^{(n)}\nu_d = \mathbf{u}_h^* \cdot \boldsymbol{\nu}$ is imposed in a weak sense, by penalization. In this way, we just need the normal vector $\boldsymbol{\nu}$ to be defined on the faces (edges for $d = 2$) of the boundary, and not on the vertices of the mesh, where it is not univocally determined.

5. Stability and discrete minimum dissipation principle

In this section, we want to analyze the properties of the numerical scheme introduced above. In particular, we investigate how the discrete formulation (21) can reproduce, mutatis mutandis, the First Law of Thermodynamics (5). This will give us information about the stability of our numerical scheme and it

will shed light on the critical terms of the discrete formulation, that may give rise to numerical instabilities. On this concern, Sec. 5.1 will be devoted to the introduction of a non-standard term to cure the onset of spurious instabilities.

Aiming at writing the discrete counterpart of the power balance (5), with the total power $\mathcal{W}$ and the Rayleigh dissipation function $\mathcal{R}$ defined as in (16) and (6), respectively, we need to introduce some discrete energetic quantities that will take part in the equation. We define the following quantities: [5]

Potential energy $\mathcal{V}^{(n)} = -\int_{\Omega^{(n)}} \mathbf{g}\cdot\mathbf{x} + \int_{\Gamma^{(n)}} \gamma + \int_{\Sigma^{(n)}} \gamma_l + \int_{\Sigma_g^{(n)}} \gamma_g$,

Kinetic energy $\mathcal{K}^{(n)} = \frac{1}{2}\int_{\Omega^{(n)}} |\mathbf{u}^{(n)}|^2$,

Dissipation function $\mathcal{R}^{(n)} = \frac{1}{2}\int_{\Omega^{(n)}} 2\nu|D(\mathbf{u}^{(n)})|^2 + \frac{1}{2}\int_{\Sigma^{(n)}} \beta|\Pi_{\Sigma^{(n)}}\mathbf{u}^{(n)}|^2 + \frac{1}{2}C_s h^2 \sum_{K\in\mathcal{T}_h^{(n)}} \int_K |\nabla p^{(n)}|^2$,

where, compared to its continuous counterpart $\mathcal{R}$ defined in (6), the discrete dissipation function contains also the "viscous" contribution of the pressure stabilization term included in $s_p^{(n)}$ (cf. (22)). With this notation, we can write a discrete counterpart of the First Law of Thermodynamics (5), as stated in the following result:

Theorem 1. *Let $(\mathbf{u}^{(n)}, p^{(n)})$, $n = 0,\dots,N$ be the solution of the discrete problem (21) – with the stabilization term (22) – and let $\mathbf{V}^{(n)}$, $n = 0,\dots,N$ be the domain velocity defined by problem (24), with the explicit choice (25), i.e. $\mathbf{u}^* = \mathbf{u}^{(n)}$. Then, the following balance holds:*

$$\begin{aligned}\int_{\Sigma_b} \boldsymbol{\zeta}\cdot\mathbf{u}^{(n+1)} - \frac{\mathcal{V}^{(n+2)}-\mathcal{V}^{(n+1)}}{\Delta t} - \frac{\mathcal{K}^{(n+1)}-\mathcal{K}^{(n)}}{\Delta t} - \int_{\Sigma_b}\left(\frac{1}{2}|\mathbf{u}^{(n+1)}|^2\mathbf{u}^{(n)}\cdot\boldsymbol{\nu} - \mathbf{g}\cdot\mathbf{x}\,\mathbf{u}^{(n+1)}\cdot\boldsymbol{\nu}\right)\\ = 2\mathcal{R}^{(n+1)} + \frac{1}{2\Delta t}\int_{\Omega^{(n)}} |\mathbf{u}^{(n+1)}\circ\mathcal{A}_{n,n+1} - \mathbf{u}^{(n)}|^2\\ - \varepsilon_g^{(n+1)} - \varepsilon_{\Gamma,expl}^{(n+1)} + \Phi_{expl}^{(n+1)},\end{aligned} \tag{27}$$

where

$$\begin{aligned}\varepsilon_g^{(n+1)} &= -\frac{\Delta t}{2}\int_{\partial\Omega^{(n+1)}} (v^{(n+1)})^2\mathbf{g}\cdot\boldsymbol{\nu},\\ \varepsilon_{\Gamma,expl}^{(n+1)} &= \frac{\gamma}{\Delta t}\left(|\Gamma^{(n+2)}| - |\Gamma^{(n+1)}| - \Delta t\int_{\Gamma^{(n+1)}} \mathrm{div}_\Gamma\mathbf{V}^{(n+1)}\right),\\ \Phi_{expl}^{(n+1)} &= \int_{\Gamma^{(n+1)}} \gamma\,\mathrm{div}_\Gamma(\mathbf{u}^{(n+1)} - \mathbf{V}^{(n+1)}) + \int_{\Omega^{(n+1)}} \mathbf{g}\cdot\mathbf{x}\,\mathrm{div}\,\mathbf{u}^{(n+1)}.\end{aligned}$$

If, instead, the implicit kinematic condition (26) is chosen – namely $\mathbf{u}^* = \mathbf{u}^{(n+1)}\circ\mathcal{A}_{n,n+1}$ – the balance reads

$$\begin{aligned}\int_{\Sigma_b} \boldsymbol{\zeta}\cdot\mathbf{u}^{(n+1)} - \frac{\mathcal{V}^{(n+1)}-\mathcal{V}^{(n)}}{\Delta t} - \frac{\mathcal{K}^{(n+1)}-K^{(n)}}{\Delta t} - \int_{\Sigma_b}\left(\frac{1}{2}|\mathbf{u}^{(n+1)}|^2\mathbf{u}^{(n)}\cdot\boldsymbol{\nu} - \mathbf{g}\cdot\mathbf{x}\,\mathbf{u}^{(n+1)}\cdot\boldsymbol{\nu}\right)\\ = 2\mathcal{R}^{(n+1)} + \frac{1}{2\Delta t}\int_{\Omega^{(n)}} |\mathbf{u}^{(n+1)}\circ\mathcal{A}_{n,n+1} - \mathbf{u}^{(n)}|^2\\ + \varepsilon_g^{(n)} + \varepsilon_{\Gamma,impl}^{(n)} + \Phi_{impl}^{(n+1)},\end{aligned} \tag{28}$$

where

$$\begin{aligned}\varepsilon_g^{(n)} &= -\frac{\Delta t}{2}\int_{\partial\Omega^{(n)}} (v^{(n)})^2\mathbf{g}\cdot\boldsymbol{\nu},\\ \varepsilon_{\Gamma,impl}^{(n)} &= -\frac{\gamma}{\Delta t}\left(|\Gamma^{(n+1)}| - |\Gamma^{(n)}| - \Delta t\int_{\Gamma^{(n+1)}} \mathrm{div}_\Gamma(\mathbf{V}^{(n)}\circ\mathcal{A}_{n,n+1}^{-1})\right),\\ \Phi_{impl}^{(n+1)} &= \int_{\Gamma^{(n+1)}} \gamma\,\mathrm{div}_\Gamma(\mathbf{u}^{(n+1)} - \mathbf{V}^{(n)}\circ\mathcal{A}_{n,n+1}^{-1}) + \int_{\Omega^{(n+1)}} \mathbf{g}\cdot\mathbf{x}\,\mathrm{div}\,\mathbf{u}^{(n+1)}.\end{aligned}$$

[5] For simplicity, from now on the subscript h will be understood, though we will always refer to fully discrete quantities.

The proof of these results employs some properties stemming from the particular choice for the domain velocity $\mathbf{V}^{(n)}$. We collect such properties in the following statement, whose proof for the 3D case can be found in [15], and easily generalized to the case $d = 2$. [6]

Proposition 2. *Let $\mathbf{V}^{(n)} : \Omega^{(n)} \to \mathbb{R}^d$ be the domain velocity at time $t^{(n)}$, such that $\Omega^{(n+1)} = (I + \Delta t\, \mathbf{V}^{(n)})(\Omega^{(n)})$, and assume that there exists $i \in \{1, \dots, d\}$ s.t. $\mathbf{V}^{(n)} = v^{(n)}\, \mathbf{e}_i$. Then, for any function $\varphi : \Omega^{(n+1)} \to \mathbb{R}$, the* Geometric Conservation Law *(GCL) holds, in the following two formulations:*

$$\int_{\Omega^{(n+1)}} \varphi - \int_{\Omega^{(n)}} \varphi \circ \mathcal{A}_{n,n+1} = \Delta t \int_{\Omega^{(n+1)}} \varphi \operatorname{div}(\mathbf{V}^{(n)} \circ \mathcal{A}^{-1}_{n,n+1}), \tag{29a}$$

$$\int_{\Omega^{(n+1)}} \varphi - \int_{\Omega^{(n)}} \varphi \circ \mathcal{A}_{n,n+1} = \Delta t \int_{\Omega^{(n)}} \varphi \circ \mathcal{A}_{n,n+1} \operatorname{div} \mathbf{V}^{(n)}. \tag{29b}$$

Moreover, let φ be nonnegative, and Δt sufficiently small, such that $1 + \Delta t \operatorname{div}_\Gamma \mathbf{V}^{(n)} \geq 0$ on $\Gamma^{(n+1)}$ and $1 - \Delta t \operatorname{div}_\Gamma(\mathbf{V}^{(n)} \circ \mathcal{A}^{-1}_{n,n+1}) \geq 0$ on $\Gamma^{(n+1)}$. Then, the Surface Geometric Conservation Laws *(SGCL) hold:*

$$\int_{\Gamma^{(n+1)}} \varphi - \int_{\Gamma^{(n)}} \varphi \circ \mathcal{A}_{n,n+1} \geq \Delta t \int_{\Gamma^{(n)}} \varphi \circ \mathcal{A}_{n,n+1}\ \operatorname{div}_\Gamma \mathbf{V}^{(n)}, \tag{30a}$$

$$\int_{\Gamma^{(n+1)}} \varphi - \int_{\Gamma^{(n)}} \varphi \circ \mathcal{A}_{n,n+1} \leq \Delta t \int_{\Gamma^{(n+1)}} \varphi\ \operatorname{div}_\Gamma(\mathbf{V}^{(n)} \circ \mathcal{A}^{-1}_{n,n+1}). \tag{30b}$$

Hinging upon these results, we can show how to derive the discrete balances of Thm. 1.

Proof of Theorem 1. Taking $\mathbf{v} = \mathbf{u}^{(n+1)} \circ \mathcal{A}_{n,n+1}, \pi = p^{(n+1)} \circ \mathcal{A}_{n,n+1}$ in (21), we get

$$\begin{aligned}
&2\frac{\mathcal{K}^{(n+1)}}{\Delta t} + \int_{\Omega^{(n+1)}} 2\nu |D(\mathbf{u}^{(n+1)})|^2 + \int_{\Sigma^{(n+1)}} \beta |\mathbf{u}^{(n+1)}|^2 + C_s h^2 \sum_{K \in \mathcal{T}_h^{(n+1)}} \int_K |\nabla p^{(n+1)}|^2 \\
&\quad + \int_{\Omega^{(n+1)}} \left[\frac{1}{2} (\mathbf{u}^{(n)} - \mathbf{V}^{(n)}) \cdot \nabla |\mathbf{u}^{(n+1)}|^2 - |\mathbf{u}^{(n+1)}|^2 \operatorname{div} \mathbf{V}^{(n)} \right] \\
&\quad + \frac{1}{2} \int_{\Omega^{(n+1)}} |\mathbf{u}^{(n+1)}|^2 \operatorname{div} \mathbf{u}^{(n)} - \frac{1}{2} \int_{\Gamma^{(n+1)}} |\mathbf{u}^{(n+1)}|^2 (\mathbf{u}^{(n)} - \mathbf{V}^{(n)}) \cdot \boldsymbol{\nu} \\
&= \frac{1}{\Delta t} \int_{\Omega^{(n)}} \mathbf{u}^{(n)} \cdot \mathbf{u}^{(n+1)} + \int_{\Omega^{(n+1)}} \mathbf{g} \cdot \mathbf{u}^{(n+1)} + \int_{\Sigma_b} \boldsymbol{\zeta} \cdot \mathbf{u}^{(n+1)} \\
&\quad - \int_{\Gamma^{(n+1)}} \gamma \operatorname{div}_\Gamma \mathbf{u}^{(n+1)} + \int_{\partial\Gamma^{(n+1)}} \gamma \cos\theta_s\ \mathbf{u}^{(n+1)} \cdot \mathbf{b}_s,
\end{aligned} \tag{31}$$

where the bulk divergence terms canceled out due to the particular choice of the test functions. Now, for the advection term we have

$$\begin{aligned}
&\frac{1}{2} \int_{\Omega^{(n+1)}} (\mathbf{u}^{(n)} - \mathbf{V}^{(n)}) \cdot \nabla |\mathbf{u}^{(n+1)}|^2 \\
&= -\frac{1}{2} \int_{\Omega^{(n+1)}} |\mathbf{u}^{(n+1)}|^2 (\operatorname{div} \mathbf{u}^{(n)} - \operatorname{div} \mathbf{V}^{(n)}) + \frac{1}{2} \int_{\Gamma^{(n+1)}} |\mathbf{u}^{(n+1)}|^2 (\mathbf{u}^{(n)} - \mathbf{V}^{(n)}) \cdot \boldsymbol{\nu} + \frac{1}{2} \int_{\Sigma_b} |\mathbf{u}^{(n+1)}|^2 \mathbf{u}^{(n)} \cdot \boldsymbol{\nu},
\end{aligned}$$

[6] The results contained in Prop. 2 also hold if just the time discretization is considered. Indeed, the proof makes no use of the space discretization.

while for the explicit part of the Euler time derivative approximation we can write

$$\begin{aligned}\frac{1}{\Delta t}\int_{\Omega^{(n)}}\mathbf{u}^{(n)}\cdot\mathbf{u}^{(n+1)} &= \frac{1}{\Delta t}\int_{\Omega^{(n)}}\mathbf{u}^{(n)}\cdot\mathbf{u}^{(n+1)}\circ\mathcal{A}_{n,n+1}\\ &= \frac{\mathcal{K}^{(n)}}{\Delta t}+\frac{1}{2\Delta t}\int_{\Omega^{(n)}}|\mathbf{u}^{(n+1)}\circ\mathcal{A}_{n,n+1}|^2-\frac{1}{2\Delta t}\int_{\Omega^{(n)}}|\mathbf{u}^{(n+1)}\circ\mathcal{A}_{n,n+1}-\mathbf{u}^{(n)}|^2\\ &\overset{(\mathrm{GCL})}{=}\frac{\mathcal{K}^{(n)}}{\Delta t}+\frac{\mathcal{K}^{(n+1)}}{\Delta t}-\frac{1}{2}\int_{\Omega^{(n+1)}}|\mathbf{u}^{(n+1)}|^2\mathrm{div}\,\mathbf{V}^{(n)}-\frac{1}{2\Delta t}\int_{\Omega^{(n)}}|\mathbf{u}^{(n+1)}\circ\mathcal{A}_{n,n+1}-\mathbf{u}^{(n)}|^2,\end{aligned}$$

where in the last line, we have used the GCL (29b). Being $\mathbf{g}=-g\mathbf{e}_d=-g\nabla x_d$, we can also rewrite the gravity term as follows:

$$\int_{\Omega^{(n+1)}}\mathbf{g}\cdot\mathbf{u}^{(n+1)}=-\int_{\Omega^{(n+1)}}g\nabla x_d\cdot\mathbf{u}^{(n+1)}=-\int_{\Omega^{(n+1)}}\mathbf{g}\cdot\mathbf{x}\;\mathrm{div}\,\mathbf{u}^{(n+1)}+\int_{\partial\Omega^{(n+1)}}\mathbf{g}\cdot\mathbf{x}\;\mathbf{u}^{(n+1)}\cdot\boldsymbol{\nu}.$$

Combining all the relations developed so far in the proof, some terms of (31) cancel out, resulting in the following intermediate identity:

$$\begin{aligned}&\frac{\mathcal{K}^{(n+1)}-\mathcal{K}^{(n)}}{\Delta t}+\int_{\Omega^{(n+1)}}2\nu|D(\mathbf{u}^{(n+1)})|^2+\int_{\Sigma^{(n+1)}}\beta|\mathbf{u}^{(n+1)}|^2+C_sh^2\sum_{K\in\mathcal{T}_h^{(n+1)}}\int_K|\nabla p^{(n+1)}|^2\\ &\qquad+\frac{1}{2}\int_{\Sigma_b}|\mathbf{u}^{(n+1)}|^2\mathbf{u}^{(n)}\cdot\boldsymbol{\nu}+\frac{1}{2\Delta t}\int_{\Omega^{(n)}}|\mathbf{u}^{(n+1)}\circ\mathcal{A}_{n,n+1}-\mathbf{u}^{(n)}|^2\\ &=-\int_{\Omega^{(n+1)}}\mathbf{g}\cdot\mathbf{x}\;\mathrm{div}\,\mathbf{u}^{(n+1)}+\int_{\partial\Omega^{(n+1)}}\mathbf{g}\cdot\mathbf{x}\;\mathbf{u}^{(n+1)}\cdot\boldsymbol{\nu}+\int_{\Sigma_b}\boldsymbol{\zeta}\cdot\mathbf{u}^{(n+1)}\\ &\qquad-\int_{\Gamma^{(n+1)}}\gamma\,\mathrm{div}_{\Gamma}\mathbf{u}^{(n+1)}+\int_{\partial\Gamma^{(n+1)}}\gamma\,\cos\theta_s\;\mathbf{u}^{(n+1)}\cdot\mathbf{b}_s.\end{aligned}\tag{32}$$

Now, we need to operate on the gravitational terms in (32). Aiming at connecting them with the discrete time derivative of the gravitational potential energy, we initially consider the case in which the explicit choice (25) is made for the kinematic condition on $\Gamma^{(n+1)}$. Under this choice, we can use the GCL (29b) to rewrite the time increment of the gravity potential:

$$\begin{aligned}&\frac{1}{\Delta t}\left(\int_{\Omega^{(n+2)}}\mathbf{g}\cdot\mathbf{x}-\int_{\Omega^{(n+1)}}\mathbf{g}\cdot\mathbf{x}\right)\\ &\overset{(\mathrm{GCL})}{=}\frac{1}{\Delta t}\int_{\Omega^{(n+1)}}\mathbf{g}\cdot(\mathbf{x}\circ\mathcal{A}_{n+1,n+2}-\mathbf{x})+\int_{\Omega^{(n+1)}}\mathbf{g}\cdot\mathbf{x}\circ\mathcal{A}_{n+1,n+2}\;\mathrm{div}\,\mathbf{V}^{(n+1)}\\ &=\int_{\Omega^{(n+1)}}\mathbf{g}\cdot\mathbf{V}^{(n+1)}+\int_{\Omega^{(n+1)}}\mathbf{g}\cdot\mathbf{x}\;\mathrm{div}\,\mathbf{V}^{(n+1)}+\Delta t\int_{\Omega^{(n+1)}}\mathbf{g}\cdot\mathbf{V}^{(n+1)}\;\mathrm{div}\,\mathbf{V}^{(n+1)}\\ &=-\int_{\Omega^{(n+1)}}g\partial_{x_d}\left(x_d\,v^{(n+1)}\right)-\frac{\Delta t}{2}\int_{\Omega^{(n+1)}}g\partial_{x_d}(v^{(n+1)})^2\\ &=\int_{\partial\Omega^{(n+1)}}\mathbf{g}\cdot\mathbf{x}\;\mathbf{V}^{(n+1)}\cdot\boldsymbol{\nu}-\frac{\Delta t}{2}\int_{\partial\Omega^{(n+1)}}g(v^{(n+1)})^2\nu_d.\end{aligned}\tag{33}$$

Recalling the kinematic condition, it is possible to replace every instance of $\mathbf{V}^{(n+1)}\cdot\boldsymbol{\nu}$ on the free surface $\Gamma^{(n+1)}$ with the fluid normal velocity $\mathbf{u}^{(n+1)}\cdot\boldsymbol{\nu}$. Moreover, being $\mathbf{V}^{(n+1)}\cdot\boldsymbol{\nu}=0$, $\mathbf{u}^{(n+1)}\cdot\boldsymbol{\nu}=0$ on $\Sigma^{(n+1)}$, and since the normal vector of $\Gamma^{(n+1)}$ and $\Sigma^{(n+1)}$ can be assumed linearly independent, we can also state that $\mathbf{V}^{(n+1)}\cdot\mathbf{b}_s=\mathbf{u}^{(n+1)}\cdot\mathbf{b}_s$ at $\partial\Gamma^{(n+1)}=\overline{\Gamma^{(n+1)}}\cap\overline{\Sigma^{(n+1)}}$. Therefore, adding $\frac{\mathcal{V}^{(n+2)}-\mathcal{V}^{(n+1)}}{\Delta t}$ to both sides of (32), employing (33) and rearranging the terms provides (27): the ε-terms and $\Phi_{expl}^{(n+1)}$ are originated simply from this rearrangement.

To conclude the proof, an analogous argument can be employed to show (28), stemming from the enforcement of the kinematic condition (26), which entails the following reformulation of the discrete time derivative of the gravity potential:

$$
\begin{aligned}
&\frac{1}{\Delta t}\left(\int_{\Omega^{(n+1)}} \mathbf{g}\cdot\mathbf{x} - \int_{\Omega^{(n)}} \mathbf{g}\cdot\mathbf{x}\right) \\
&\overset{(29a)}{=} \frac{1}{\Delta t}\int_{\Omega^{(n)}} \mathbf{g}\cdot(\mathbf{x}\circ\mathcal{A}_{n,n+1}-\mathbf{x}) + \int_{\Omega^{(n+1)}} \mathbf{g}\cdot\mathbf{x}\,\operatorname{div}(\mathbf{V}^{(n)}\circ\mathcal{A}_{n,n+1}^{-1}) \\
&= \int_{\Omega^{(n)}} \mathbf{g}\cdot\mathbf{V}^{(n)} - \int_{\Omega^{(n+1)}} \mathbf{g}\cdot(\mathbf{V}^{(n)}\circ\mathcal{A}_{n,n+1}^{-1}) + \int_{\partial\Omega^{(n+1)}} \mathbf{g}\cdot\mathbf{x}\,(\mathbf{V}^{(n)}\circ\mathcal{A}_{n,n+1}^{-1})\cdot\boldsymbol{\nu} \\
&\overset{(29b)}{=} -\Delta t\int_{\Omega^{(n)}} \mathbf{g}\cdot\mathbf{V}^{(n)}\,\operatorname{div}\mathbf{V}^{(n)} + \int_{\partial\Omega^{(n+1)}} \mathbf{g}\cdot\mathbf{x}\,(\mathbf{V}^{(n)}\circ\mathcal{A}_{n,n+1}^{-1})\cdot\boldsymbol{\nu} \\
&= \frac{\Delta t}{2}\int_{\Omega^{(n)}} g\partial_{x_d}(v^{(n)})^2 + \int_{\partial\Omega^{(n+1)}} \mathbf{g}\cdot\mathbf{x}\,(\mathbf{V}^{(n)}\circ\mathcal{A}_{n,n+1}^{-1})\cdot\boldsymbol{\nu} \\
&= \frac{\Delta t}{2}\int_{\partial\Omega^{(n)}} g(v^{(n)})^2\nu_d + \int_{\partial\Omega^{(n+1)}} \mathbf{g}\cdot\mathbf{x}\,(\mathbf{V}^{(n)}\circ\mathcal{A}_{n,n+1}^{-1})\cdot\boldsymbol{\nu}.
\end{aligned}
$$

□

Some remarks are now due in order to interpret the results of Thm. 1.

- The left-hand sides of both (27) and (28) are discrete versions of the total power $\mathcal{W}$ as written in (16): they contain the contribution of the external stress $\boldsymbol{\zeta}$ and the time variations of the potential and kinetic energy, together with their flux through the open boundary Σ_b.
- The right-hand sides of the balances (27) and (28) contain the discrete counterpart $\mathcal{R}^{(n+1)}$ of the Rayleigh dissipation function $\mathcal{R}$ introduced in (6). However, some additional terms are also present, whose origin is strictly numerical: the next points intend to discuss them.
- The Euler dissipation term $\frac{1}{2\Delta t}\int_{\Omega^{(n)}} |\mathbf{u}^{(n+1)}\circ\mathcal{A}_{n,n+1}-\mathbf{u}^{(n)}|^2$ is generated by the discretization of the time derivative. Being it nonnegative, it is a further source of dissipation, so it does not bring spurious power into the system and does not need to be controlled by any stabilization term.
- Employing (30) with $\varphi = 1$, we see that both $\varepsilon_{\Gamma,expl}^{(n+1)}$ and $\varepsilon_{\Gamma,impl}^{(n)}$ are positive, for Δt sufficiently small. Hence, further numerical dissipation is introduced in the balance (28), whereas spurious power is generated in (27), where $\varepsilon_{\Gamma,expl}^{(n+1)}$ appears with the opposite sign. In this latter case, instabilities may arise, and in Sec. 5.1 we will show a way to cope with them.
- Being the normal component of the domain velocity zero on $\partial\Omega^{(n)}\setminus\Gamma^{(n)}$, the gravity spurious power can be rewritten as $\varepsilon_g^{(n)} = -\frac{\Delta t}{2}\int_{\Gamma^{(n)}}(v^{(n+1)})^2\mathbf{g}\cdot\boldsymbol{\nu}$. Therefore, $\varepsilon_g^{(n)}$ is positive at any time $t^{(n)}$ if, e.g., the free surface is the graph of a function, so that $\mathbf{g}\cdot\boldsymbol{\nu} < 0$ on $\Gamma^{(n)}$. In such a situation, we can comment the contribution of this term in a similar way to the previous point: the term under inspection is another dissipation source in (28), whereas it brings spurious power generation in the balance (27).
- Unfortunately, we cannot say anything about the sign of $\Phi_{expl}^{(n)}$ and $\Phi_{impl}^{(n)}$. However, in Sec. 6 we will show that these two terms do not practically spoil the evolution of the simulated phenomenon, neither they affect the stabilizing effect of the additional term that we are going to introduce in Sec. 5.1.

5.1. A remedy to surface instabilities

Motivated by the considerations drawn after Thm. 1, the present section is devoted to the introduction of a stabilization term that can compensate the instable contributions of the spurious terms that appear in the balance (27). Indeed, we saw that this issue characterizes the explicit treatment of the geometry,

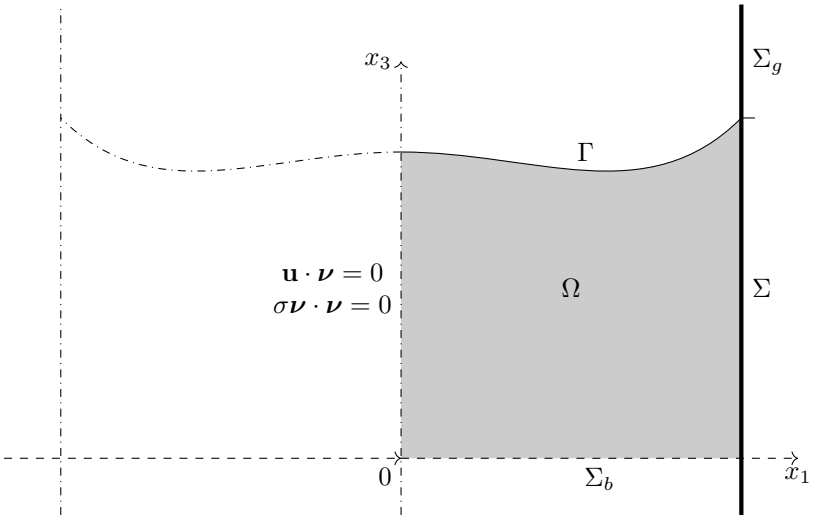

Figure 2: Axisymmetric computational domain Ω (gray area).

resulting from the choice (25) in the kinematic condition. In particular, we focus on the stabilization of $\varepsilon^{(n+1)}_{\Gamma,expl}$.

Remark 8. Referring to the considerations of the previous section, in principle one should look also for a stabilization of the gravity term $\varepsilon^{(n+1)}_g$. However, we will see in the numerical results of Sec. 6.2.2 that the actual source of instabilities is only the free-surface term $\varepsilon^{(n+1)}_{\Gamma,expl}$. This is in line with the results of [15], where numerical results showed that the instable contribution of the gravity spurious term is generally compensated by the Euler dissipation term. Anyway, for the sake of completeness, we remark that adding the form

$$\Delta t\, S^{(n+1)}_g(\mathbf{u}^{(n+1)},\mathbf{v}) = -\frac{\Delta t}{2}\int_{\Gamma^{(n+1)}} \frac{\mathbf{u}^{(n+1)}\cdot\boldsymbol{\nu}}{\nu_d}\,\frac{\mathbf{v}\cdot\boldsymbol{\nu}}{\nu_d}\mathbf{g}\cdot\boldsymbol{\nu}$$

to the left-hand side of (21) would result in an asymptotically consistent stabilization of the scheme, which would remove $\varepsilon^{(n+1)}_g$ from balance (27).

For the ease of presentation, in the present section we consider an axisymmetric domain. That is, we refer to the shaded 2D domain depicted in Fig. 2, with the third axis $x_1 = x_2 = 0$ as the symmetry axis. On the central axis $x_1 = x_2 = 0$, the boundary conditions are prescribed by symmetry: $\mathbf{u}\cdot\boldsymbol{\nu} = 0$, $\sigma\boldsymbol{\nu}\cdot\boldsymbol{\nu} = 0$.

Our search path moves from a deeper look into the proof of the SGCL (30a), from which it is possible to derive the following result:

Corollary 1. *Let $\Omega^{(n)} \subset \mathbb{R}^3$ be such that we can assume cylindrical symmetry for the problem, with the symmetry axis along the third dimension, and let $\mathbf{V}^{(n)} = v^{(n)}\,\mathbf{e}_3$. For any sufficiently regular function $\varphi : \Gamma^{(n)} \to \mathbb{R}$ and for $\Delta t \to 0$, it holds*

$$\begin{aligned}\int_{\Gamma^{(n+1)}} \varphi\circ\mathcal{A}^{-1}_{n,n+1} - \int_{\Gamma^{(n)}}\varphi =& \Delta t\int_{\Gamma^{(n)}}\varphi\ \mathrm{div}_\Gamma\mathbf{V}^{(n)} + \frac{\Delta t^2}{2}\int_{\Gamma^{(n)}}\varphi\ \nu_3^2(\nu_1\partial_3 v^{(n)} - \nu_3\partial_1 v^{(n)})^2 \\ &- \frac{\Delta t^3}{2}\int_{\Gamma^{(n)}}\varphi\nu_1\nu_3^2(\nu_1\partial_3 v^{(n)} - \nu_3\partial_1 v^{(n)})^3 + \mathcal{O}(\Delta t^4).\end{aligned} \tag{34}$$

Proof. Taking a generic φ, we can write

$$\int_{\Gamma^{(n+1)}}\varphi\circ\mathcal{A}^{-1}_{n,n+1} = \int_{\Gamma^{(n)}}\varphi|\mathrm{cof}(\nabla\mathcal{A}_{n,n+1})\boldsymbol{\nu}|,$$

where $\mathrm{cof}(\cdot)$ denotes the cofactor matrix. Assuming cylindrical symmetry, we have that $\nu_2 = \boldsymbol{\nu}\cdot\mathbf{e}_2 = 0$, and $\partial_2 \mathbf{V}^{(n)} = \partial_2 v^{(n)}\,\mathbf{e}_3 = 0$, whence

$$\begin{aligned}\int_{\Gamma^{(n+1)}} \varphi \circ \mathcal{A}_{n,n+1}^{-1} &= \int_{\Gamma^{(n)}} \varphi|(\nu_1 + \Delta t(\nu_1\partial_3 v^{(n)} - \nu_3\partial_1 v^{(n)}), \nu_2 + \Delta t(\nu_2\partial_3 v^{(n)} - \nu_3\partial_2 v^{(n)}), \nu_3)| \\ &= \int_{\Gamma^{(n)}} \varphi\sqrt{1 + 2\Delta t\,\nu_1(\nu_1\partial_3 v^{(n)} - \nu_3\partial_1 v^{(n)}) + \Delta t^2(\nu_1\partial_3 v^{(n)} - \nu_3\partial_1 v^{(n)})^2}.\end{aligned}$$

Then, we employ Taylor expansion around $\Delta t = 0$, exploiting $|\boldsymbol{\nu}|^2 = \nu_1^2 + \nu_3^2 = 1$. Separating the different terms of the expansion and noticing that in the axisymmetric case

$$\mathrm{div}_{\,\Gamma}\mathbf{V}^{(n)} = \nu_1(\nu_1\partial_3 v^{(n)} - \nu_3\partial_1 v^{(n)})$$

yield the thesis.

□

Since the identity (34) comes from Taylor expansion, we can state that the terms on the right-hand side give indeed the first, second, and third time derivatives of the integral of φ, about the time $t^{(n)}$, from the right. Inspired by the second order term of (34), we introduce the following form:

$$S_\Gamma^{(n)}(\mathbf{u}^{(n)}, \mathbf{v}) = \frac{1}{2}\int_{\Gamma^{(n)}} \gamma\,\nu_3^2 \left(\nu_1\partial_3\frac{\mathbf{u}^{(n)}\cdot\boldsymbol{\nu}}{\nu_3} - \nu_3\partial_1\frac{\mathbf{u}^{(n)}\cdot\boldsymbol{\nu}}{\nu_3}\right)\left(\nu_1\partial_3\frac{\mathbf{v}\cdot\boldsymbol{\nu}}{\nu_3} - \nu_3\partial_1\frac{\mathbf{v}\cdot\boldsymbol{\nu}}{\nu_3}\right), \tag{35}$$

where the choice of the arguments of the partial derivatives is inspired by the kinematic condition as written in (24). Including this form in the formulation (21) yields the following problem: given $\mathbf{u}^{(0)}$, for each $n = 0, \dots, N-1$, find $(\mathbf{u}^{(n+1)}, p^{(n+1)}) \in V_h^{(n+1)} \times P_h^{(n+1)}$ such that, for all $(\mathbf{v}, \pi) \in V_h^{(n)} \times P_h^{(n)}$,

$$\begin{aligned}\frac{1}{\Delta t}(\mathbf{u}^{(n+1)}, \mathbf{v})_{\Omega^{(n+1)}} &+ a^{(n+1)}(\mathbf{u}^{(n+1)}, \mathbf{v}) + b^{(n+1)}(\mathbf{v}, p^{(n+1)}) - b^{(n+1)}(\mathbf{u}^{(n+1)}, \pi) \\ &+ c_{ALE}^{(n+1)}(\mathbf{u}^{(n)}, \mathbf{V}^{(n)}, \mathbf{u}^{(n+1)}, \mathbf{v}) + s_p^{(n+1)}(\mathbf{V}^{(n)}, \mathbf{u}^{(n)}, \mathbf{u}^{(n+1)}, \mathbf{v}, p^{(n+1)}, \pi) \\ &+ \alpha\Delta t\, S_\Gamma^{(n+1)}(\mathbf{V}^{(n+1)}, \mathbf{v}) = \frac{1}{\Delta t}(\mathbf{u}^{(n)}, \mathbf{v})_{\Omega^{(n)}} + F^{(n+1)}(\mathbf{v}).\end{aligned} \tag{36}$$

In this formulation, the term (35) is weighted by Δt, whence it is asymptotically consistent, for $\Delta t \to 0$. Moreover, we introduced the parameter α so that the new problem (36) reduces to the former, non-stabilized problem (21), when $\alpha = 0$.

At this point, we can restate the balance (27) as follows:

Theorem 2. *Let $(\mathbf{u}^{(n)}, p^{(n)})$, $n = 0, \dots, N$ be the solution of the discrete problem (36), and let $\mathbf{V}^{(n)}$, $n = 0, \dots, N$ be the domain velocity deriving from problem (24). Then, the following balance holds:*

$$\begin{aligned}&\int_{\Sigma_b} \boldsymbol{\zeta}\cdot\mathbf{u}^{(n+1)} - \frac{\mathcal{V}^{(n+2)} - \mathcal{V}^{(n+1)}}{\Delta t} - \frac{\mathcal{K}^{(n+1)} - \mathcal{K}^{(n)}}{\Delta t} - \int_{\Sigma_b}\left(\frac{1}{2}|\mathbf{u}^{(n+1)}|^2\mathbf{u}^{(n)}\cdot\boldsymbol{\nu} - \mathbf{g}\cdot\mathbf{x}\;\mathbf{u}^{(n+1)}\cdot\boldsymbol{\nu}\right) \\ &\quad = 2\mathcal{R}^{(n+1)} + \frac{1}{2\Delta t}\int_{\Omega^{(n)}} |\mathbf{u}^{(n+1)}\circ\mathcal{A}_{n,n+1} - \mathbf{u}^{(n)}|^2 \\ &\qquad - \varepsilon_g^{(n+1)} - (1-\alpha)\varepsilon_{\Gamma,expl}^{(n+1)} - \varepsilon_{\partial\Gamma,expl}^{(n+1)} + \Phi_{expl}^{(n+1)} + \alpha\Delta t^2\,\Phi_S^{(n+1)} + \alpha\,\mathcal{O}(\Delta t^3),\end{aligned} \tag{37}$$

where

$$\Phi_S^{(n+1)} = -\frac{1}{2}\int_{\Gamma^{(n+1)}} \gamma\nu_1\nu_3^2(\nu_1\partial_3 v^{(n+1)} - \nu_3\partial_1 v^{(n+1)})^3,$$

and $\varepsilon_g^{(n+1)}, \varepsilon_{\Gamma,expl}^{(n+1)}, \varepsilon_{\partial\Gamma,expl}^{(n+1)}, \Phi_{expl}^{(n+1)}$ are defined as in Thm. 1.

PROOF. Considering the expression (35) of $S_\Gamma^{(n)}$ and the explicit kinematic condition $v^{(n)}\nu_3 = \mathbf{u}^{(n)} \cdot \boldsymbol{\nu}$ on $\Gamma^{(n)}$, we can see that choosing $\mathbf{u}^{(n+1)}$ as a test function in $S_\Gamma^{(n+1)}$ yields

$$\begin{aligned} S_\Gamma^{(n+1)}(\mathbf{u}^{(n+1)}, \mathbf{u}^{(n+1)}) &= \frac{1}{2}\int_{\Gamma^{(n+1)}} \gamma\, \nu_3^2 \left(\nu_1 \partial_3 \frac{\mathbf{u}^{(n+1)} \cdot \boldsymbol{\nu}}{\nu_3} - \nu_3 \partial_1 \frac{\mathbf{u}^{(n+1)} \cdot \boldsymbol{\nu}}{\nu_3}\right)^2 \\ &= \frac{1}{2}\int_{\Gamma^{(n+1)}} \gamma\, \nu_3^2 \left(\nu_1 \partial_3 v^{(n+1)} - \nu_3 \partial_1 v^{(n+1)}\right)^2. \end{aligned}$$

Thence, if we take $\mathbf{v} = \mathbf{u}^{(n+1)}$ in (36), like we did in the proof of Thm. 1, and we collect all the free-surface terms on the same side, the following expression appears:

$$\int_{\Gamma^{(n+1)}} \gamma \mathrm{div}_\Gamma \mathbf{u}^{(n+1)} + \alpha \frac{\Delta t}{2} \int_{\Gamma^{(n+1)}} \gamma\, \nu_3^2 \left(\nu_1 \partial_3 v^{(n+1)} - \nu_3 \partial_1 v^{(n+1)}\right)^2. \tag{38}$$

Eventually, subtracting (38) from the discrete time derivative $\frac{|\Gamma^{(n+2)}| - |\Gamma^{(n+1)}|}{\Delta t}$ of the free surface measure, multiplied by γ, we can employ Cor. 1 – with $\varphi = 1$ – to obtain the thesis.

□

The present result shows that setting $\alpha = 1$ in (36) implies the substitution of the spurious, instabilizing term $\varepsilon_{\Gamma,expl}^{(n+1)}$ with new terms, in the balance. Employing Cor. 1 – with $\varphi = 1$ – we can also notice that $\varepsilon_{\Gamma,expl}^{(n+1)}$ is order one in time, while the new terms are higher order. We will see in Sec. 6.2.2 that such a modification of the scheme is actually very effective, since much larger time steps can be employed, for $\alpha = 1$, avoiding the numerical oscillation that the term $\varepsilon_{\Gamma,expl}^{(n+1)}$ would generate.

First Law of Thermodynamics and stabilization. The aptness of the proposed stabilization term can be motivated further in terms of the ability of the numerical scheme to reproduce the First Law of Thermodynamics, at the discrete level. Looking at the definitions (10) and (16) of the potential energy and the total power, we can see that the free surface appears in the First Law of Thermodynamics (13) only through the time derivative of its measure, in a term that, thanks to (8b), can be written as

$$D_t\left(\gamma|\Gamma|\right) = \int_\Gamma \gamma \mathrm{div}_\Gamma \mathbf{V}.$$

In the discrete total power at the left-hand side of (37), this terms appears as $\gamma\frac{|\Gamma^{(n+2)}| - |\Gamma^{(n+1)}|}{\Delta t}$, and the right-hand side thus contains

$$\gamma\frac{|\Gamma^{(n+2)}| - |\Gamma^{(n+1)}|}{\Delta t} - \int_{\Gamma^{(n+1)}} \gamma \mathrm{div}_\Gamma \mathbf{V}^{(n+1)} - \alpha \Delta t\, S_\Gamma^{(n+1)}(\mathbf{V}^{(n+1)}, \mathbf{V}^{(n+1)}), \tag{39}$$

which equals $(1-\alpha)\varepsilon_{\Gamma,expl}^{(n+1)} + \alpha[\Delta t^2 \Phi_S^{(n+1)} + \mathcal{O}(\Delta t^3)]$ after the application of Cor. 1. In expression (39), the first term is the first-order approximation of the time derivative of $\gamma|\Gamma|$ from the right, whereas the second one is the exact value of such a derivative, as the domain map $\mathcal{A}_{n+1,n+2}$ is linear in time for $t \in [t^{(n+1)}, t^{(n+2)}]$. Therefore, in the case $\alpha = 0$, this discrepancy gives rise to the spurious power $\varepsilon_{\Gamma,expl}^{(n+1)}$. When we switch on the stabilization by setting $\alpha = 1$, instead, we are correcting the approximation of the time derivative by means of $\Delta t S_\Gamma^{(n+1)}(\mathbf{V}^{(n+1)}, \mathbf{V}^{(n+1)})$. Indeed, comparing (35) with the Taylor expansion of Cor. 1, we notice that we are actually adding $\gamma\frac{\Delta t^2}{2}$ times the second derivative of the measure of $|\Gamma^{(n+1)}|$, which is exactly the correction that we need in order to get a higher approximation order of the time derivative of $\gamma|\Gamma^{(n+1)}|$. Thence, we can say that introducing the stabilizing form $S_\Gamma^{(n+1)}$ makes the numerical scheme more closely related to the continuous problem.

μ	$2.081 \cdot 10^{-2}$	Pa·s	radius	$4.6 \cdot 10^{-4}$	m
ρ	1115	kg/m^3	initial height	$4.6 \cdot 10^{-4}$	m
γ	$4.36 \cdot 10^{-5}$	N/m	N_1, N_3	$32, 32$	
β	66	m/s	Δt	$1 \cdot 10^{-5}$	s
θ_s	69.8°		C_s	0.4	

Table 1: Reference physical and numerical settings for Sec. 6.1.

6. Numerical results

In this section, we present some results obtained by means of the numerical scheme described and discussed in the previous sections. In particular, we adopt an explicit treatment of the domain motion, expressed by the choice (25) in the kinematic condition. The software implementation is based on the `C++ DOLFIN` interface of the `FEniCS` project [36, 37]. We are going to consider two different settings, in order to show the properties of the code and the numerical scheme itself, and to inspect the role of the different terms appearing in Thm. 1-2. Both these settings pertain to an axisymmetric 3D domain, whence we practically solve the equation – in cylindrical coordinates – in the computational domain considered in Sec. 5 and depicted in Fig. 2. In this geometry, the contact line is represented by a single point, therefore, we will be able to talk about the evolution of $\partial\Gamma$ in terms of its height and vertical velocity, which are going to be denoted by Z_{CL} and v_{CL}, respectively.

6.1. Sloshing in a capillary basin

This section is devoted to inspecting the dependence of the model on the space and time discretization. Moreover, we are going to study how the mass conservation properties of the scheme and the effect of the wall friction coefficient β are affected by the discretization. Throughout this section, we will present results for the unstabilized scheme, namely for $\alpha = 0$ in (36), but the same conclusions (not reported here) can be drawn for $\alpha = 1$. Indeed, in this test case, we are going to employ sufficiently small time steps, so that the stabilization term introduced in Sec. 5.1 is not necessary, and we can focus on other features of the numerical scheme: we postpone the numerical assessment of our stabilization and of its effectiveness to Sec. 6.2.2.

For simplicity, in this section we set an impervious wall at the boundary Σ_b, and being it distant from the free surface, we can impose no-slip boundary conditions

$$\mathbf{u} = \mathbf{0} \qquad \text{on } \Sigma_b, \tag{40}$$

instead of imposing the stress $\boldsymbol{\zeta}$ as in the previous sections. The case with Σ_b open will be the subject of Sec. 6.2.

We start with an illustrative simulation, whose physical and numerical settings are collected in Tab. 1, where N_1, N_3 denote the number of elements in the radial and axial direction, respectively. In Fig. 3 we display the evolution of the domain and the fluid velocity and pressure. The enforcement of the generalized Navier boundary condition sets a Dirac delta force at the contact line, pulling the domain upwards. Incompressibility and surface tension, then, interact with this singular load, until the equilibrium configuration of Fig. 3c is reached, with the current contact angle θ assuming the static value θ_s.

Since in the current framework mass exchange between the fluid and the environment should be prevented (cf. (40)), an interesting point to study is mass conservation. In Fig. 4a, the time evolution of the 2D computational domain area is plotted in order to display the conservation properties of the scheme. We shall recall that the ALE formulation (18) of the problem is in its non-conservative form, and moreover, the incompressibility constraint is not strongly enforced, due to the pressure stabilization introduced for the $\mathbb{P}_1 - \mathbb{P}_1$ FE choice.

Another characteristic feature of the flow at hand is the presence of the contact line $\partial\Gamma$; thus, for the rest of the section we focus on the contact line position Z_{CL} and velocity v_{CL}. Concerning their overall time evolution, from Fig. 4b we can see an exponential convergence towards the equilibrium level, at which the

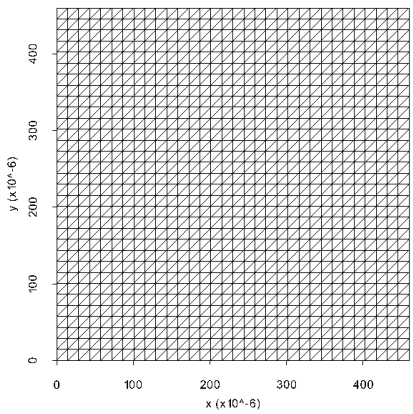

(a) initial mesh

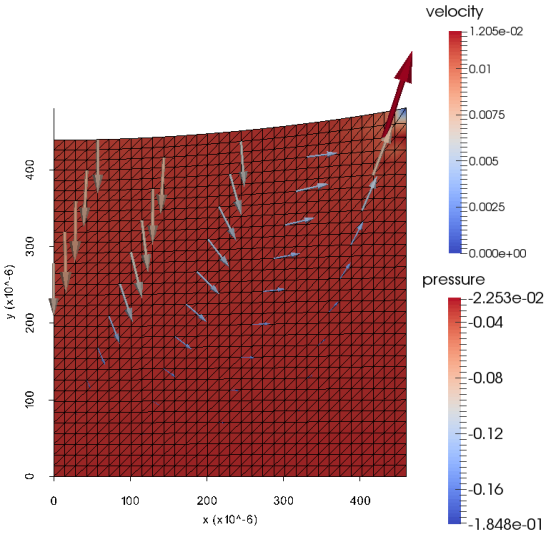

(b) $t = 0.01\,\mathrm{s}$

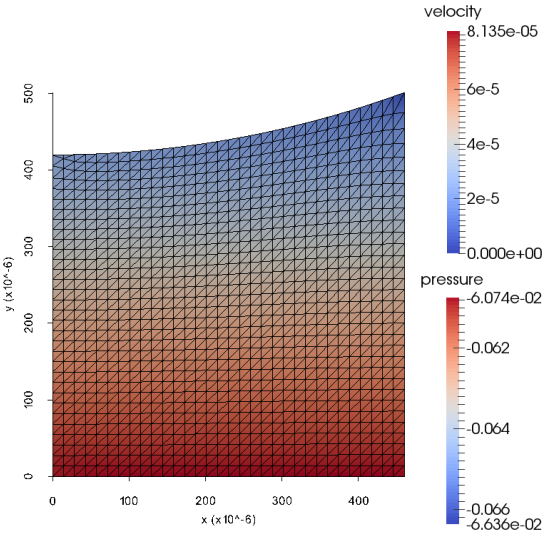

(c) $t = 0.1\,\mathrm{s}$

Figure 3: Evolution of domain, velocity and pressure.

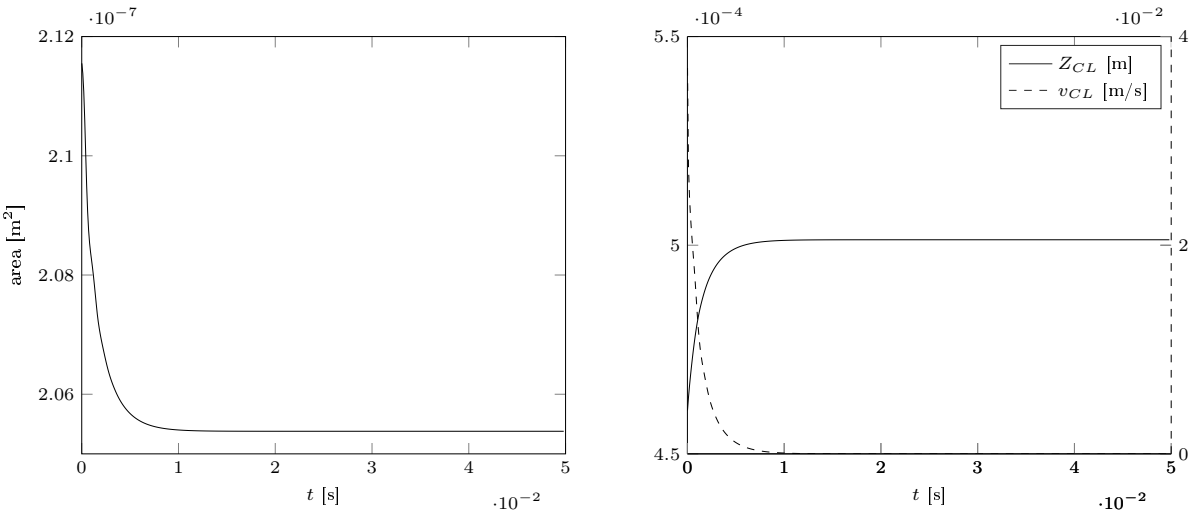

(a) Area of the domain

(b) Height (left axis) and upward velocity (right axis) of the contact line

Figure 4: Time evolution of global properties.

domain halts, and the final height is determined by the formation of the meniscus induced by the contact angle θ_s.

After the illustration of the general evolution of the system under inspection, now we want to investigate the influence of the discretization on the numerical solution. Concerning time discretization, the discussion on the stability of the scheme (cf. Sec. 5) has pointed out that there might be an upper bound for the time step Δt. This is due to the explicit treatment of the geometry (cf. (25)), whence conditional stability takes place even though implicit Euler is employed in the approximation of the fluid velocity time derivative. Indeed, performing numerical experiments we noticed that the time step has to be reduced if finer meshes are considered, in order to prevent the simulation from blowing up. Aiming at having a quantitative insight on the relation between the accuracy of the solution and the time step, we performed the simulation for different values of Δt, and we compared the final values of the contact line height (denoted by Z_{CL}^{∞}) and the transient values attained at $t = 0.006$s (denoted by $\overline{Z}_{CL}$). Employing Richardson extrapolation [38], we can compute the guesses $\widetilde{Z}_{CL}^{\infty}, \widetilde{\overline{Z}}_{CL}$ of the exact values of $Z_{CL}^{\infty}, \overline{Z}_{CL}$, respectively, and then draw the convergence plots for the relative errors $E^{\infty} = |Z_{CL}^{\infty} - \widetilde{Z}_{CL}^{\infty}|/\widetilde{Z}_{CL}^{\infty}$, $\overline{E} = |\overline{Z}_{CL} - \widetilde{\overline{Z}}_{CL}|/\widetilde{\overline{Z}}_{CL}$, w.r.t. Δt. A mesh with $N_1 = N_3 = 16$ elements in each direction is fine enough to obtain such convergence plots, reported in Fig. 5. We can see a linear order with respect to the time step, for both the final configuration and the transient. Anyway, in all the cases, the errors are so small that drawing the plots of Fig. 4b for the different values of Δt would result in having practically overlapping lines. For this reason, we decide not to report those plots.

Now, we turn towards the investigation of the effects of space discretization. As one can see in advance, by comparing the convergence plots of Fig. 5 with those of Fig. 7, the error due to time discretization is smaller than the one introduced by space discretization, in particular for the transient values. Hence we are going to fix $\Delta t = 5 \cdot 10^{-6}$s for the rest of the present section, while different space refinement strategies are going to be examined. At first, we consider a uniform space refinement, that is we perform the simulation on a sequence of meshes where the number N_1 of elements along the radial direction x_1 (cf. Fig. 2) and the number N_3 of elements along the axial direction x_3 are held equal. The time evolutions of Z_{CL} for different discretization levels are reported in Fig. 6a. We can see that the mesh has a major effect on the characteristic time of the transient: finer meshes cause a faster achievement of the equilibrium state. This suggests that the mesh has an actual effect on the *physics* governing the phenomenon. In order to further

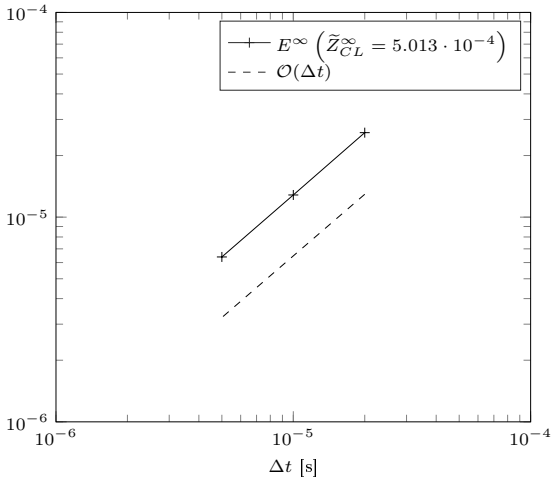

(a) Relative error E^∞ on the final value of Z_{CL}

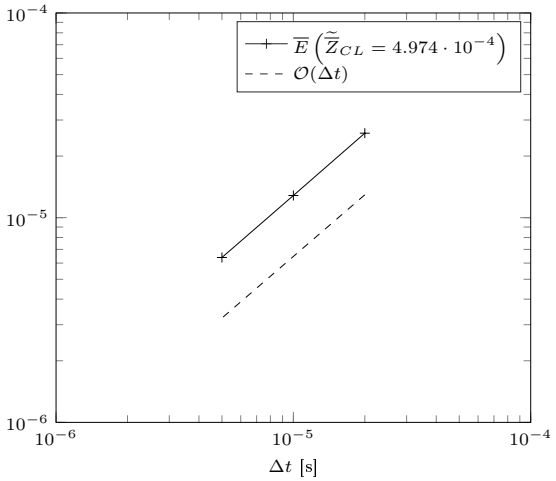

(b) Relative error $\overline{E}$ on the value of Z_{CL} at $t = 0.006$s

Figure 5: Convergence plots for Z_{CL} w.r.t. time discretization.

inspect this issue, we can turn back to the model equations (3): all the quantities and parameters of the model have a precise and uniquely defined physical meaning, except for the friction coefficient β. This observation was done also in [4], where an adimensional, mesh-independent parameter χ was introduced, related to the friction coefficient by $\beta = \frac{\mu}{\chi h_3}$, where h_3 is the discretization step in the axial direction. Therefore, we may look for the same relationship also in our scheme, holding χ constant while refining along the sole axial direction. The results of such an anisotropic refinement strategy, where we held $N_1 = 32$ fixed, are reported in Fig. 6b: indeed, scaling β with $1/h_3$ makes the different evolution plots shown therein very similar to one another. For completeness, we also checked that the effective friction coefficient β is unrelated to the *radial* discretization step. In Fig. 6c, we report the results for a sequence of meshes with different numbers N_1 of radial elements, but with N_3 and hence β held fixed. Indeed, an essential independence of the contact line evolution w.r.t. N_1 is evident. After these considerations, we can take into account uniform refinements once again, this time with a proper correction of the friction coefficient, in order to validate the scaling introduced for the friction coefficient (cf. Fig. 6d). Indeed, differently from Fig. 6a, the results reported in Fig. 6d show that the physics governing the phenomenon is substantially independent of the mesh, when β is properly scaled.

Analogously to the case of time discretization, also convergence w.r.t. the space discretization has been studied. Fig. 7 shows the convergence plots of Z_{CL}^∞ and $\overline{Z}_{CL}$ towards their Richardson extrapolations, in the case of the uniform refinement of Fig. 6d. In Fig. 7a we can see a quadratic convergence for the numerical error E^∞, whilst in Fig. 7b a sublinear order is observed for the error $\overline{E}$. This discrepancy can be related to the fact that Z_{CL}^∞ is physically prescribed by the contact angle θ_s, thus independently of β, whereas the transient values are affected by the choice of the friction coefficient. Therefore, the adopted scaling of β may not be sufficient to completely remove the modeling error, that seems to spoil the convergence behavior of $\overline{E}$.

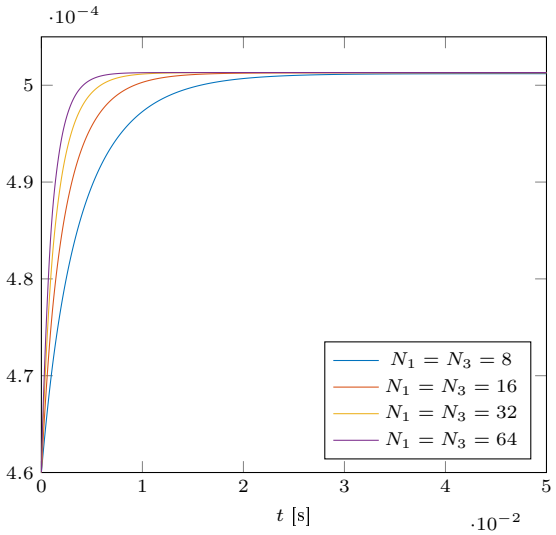

(a) $\beta = 66,\ N_1 = N_3$

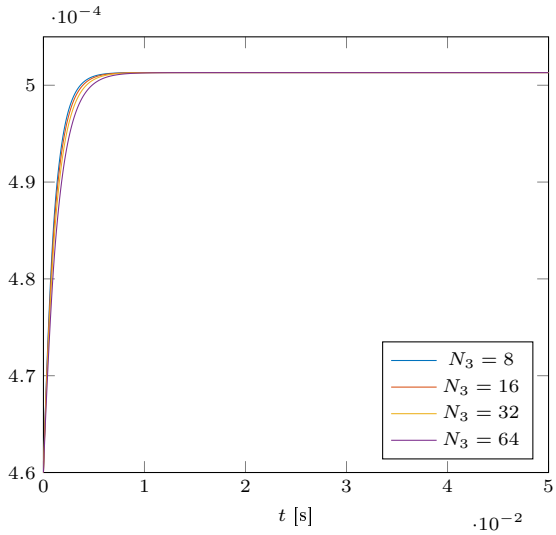

(b) $N_1 = 32,\ 1/\chi = \beta h_3 = constant$

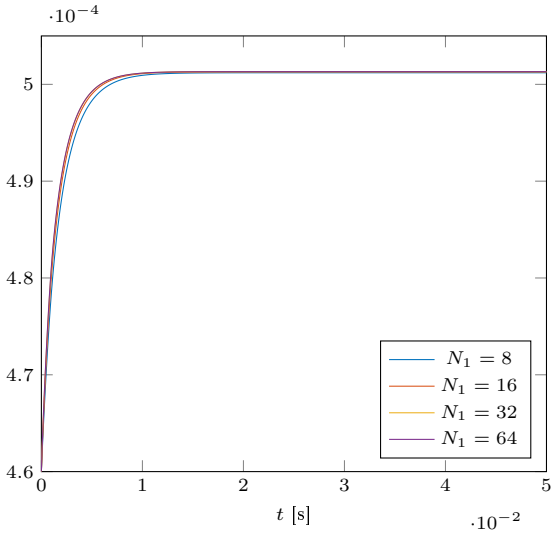

(c) $\beta = 66,\ N_3 = 32$

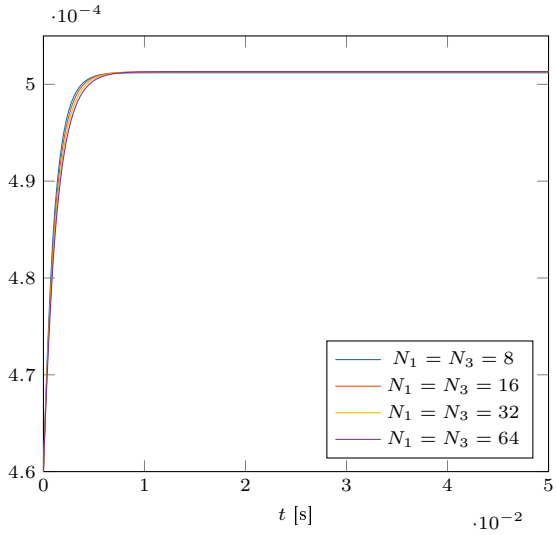

(d) $N_1 = N_3, 1/\chi = \beta h_3 = constant$

Figure 6: Dependence of Z_{CL} time evolution w.r.t. β and the space discretization parameters.

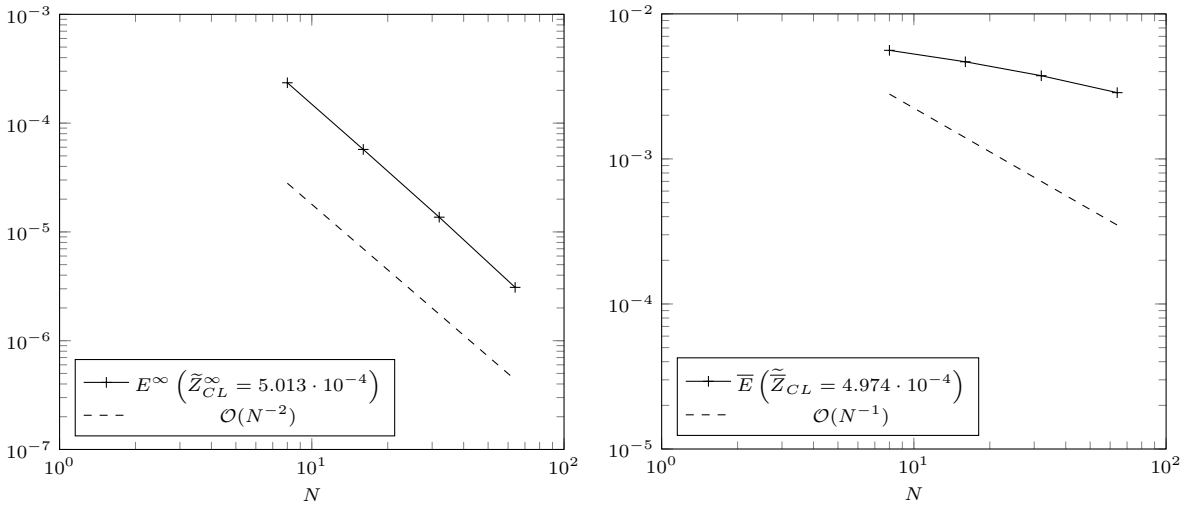

(a) Final value E^{∞}

(b) Transient value $\overline{E}$ at $t = 0.006$s

Figure 7: Convergence plots of the relative error for the contact line height w.r.t. the number of elements in each direction ($N_1 = N_3$).

6.2. Filling of a capillary pipe

In this section, we want to continue the validation of our numerical scheme, through the comparison with the experimental results reported in [4]. To this aim, a proper calibration of the friction coefficient β will be addressed. Moreover, we are going to inspect the role of the terms in the balances (27) and (37), including the effects of the stabilization term of the form $S_{\Gamma}^{(n)}$, defined in (35). In order to highlight the role of such a stabilization term, at first (Sec. 6.2.1) we present the results that can be obtained without it, namely with $\alpha = 0$ in (36); afterwards (Sec. 6.2.2), we discuss the benefits of its introduction. The physical and numerical settings of the simulations are collected in Tab. 2.

6.2.1. Results without the stabilization term S_{Γ}

In order to give a qualitative description of the fluid evolution, Fig. 8 displays the configuration of the domain section at different time steps, together with the fluid velocity and pressure fields, for the parameters set reported in Tab. 2. As one can see, in the present settings, the fluid column is pulled upwards at the contact line $\partial\Gamma$, due to the current contact angle θ being larger than the static value θ_s, while the gravity field opposes to this motion. During the evolution, the domain stretches significantly in the vertical direction: this is why we employed a number N_3 of axial elements that is larger than N_1. Eventually, the static configuration is approached without oscillations, due to the high value of β.

As already pointed out in Sec. 6.1, the friction coefficient is not rigorously defined in terms of the physical properties of the system at hand, and hence the first issue we address is the calibration of β, in order to adjust the model to the physical phenomenon that we want to simulate. In Fig. 9, we report the different histories

μ	$2.081 \cdot 10^{-2}$	Pa·s	radius	$4.6 \cdot 10^{-4}$	m
ρ	1115	kg/m^3	initial height	$4.6 \cdot 10^{-4}$	m
γ	$4.36 \cdot 10^{-5}$	N/m	N_1, N_3	$16, 80$	
β	66	m/s	Δt	$2 \cdot 10^{-5}$	s
θ_s	$69.8°$		C_s	0.4	
$\lvert\boldsymbol{\zeta}\rvert = \boldsymbol{\zeta} \cdot \mathbf{e}_3$	$4.51 \cdot 10^{-3}$	m^2/s^2			

Table 2: Physical and numerical settings for Sec. 6.2.

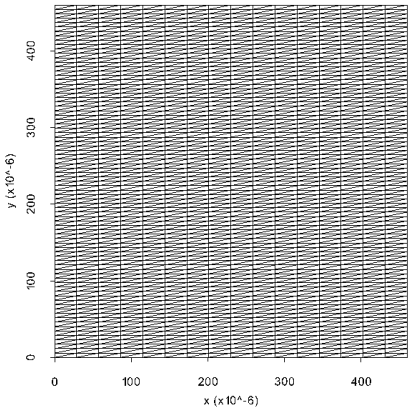

(a) initial mesh

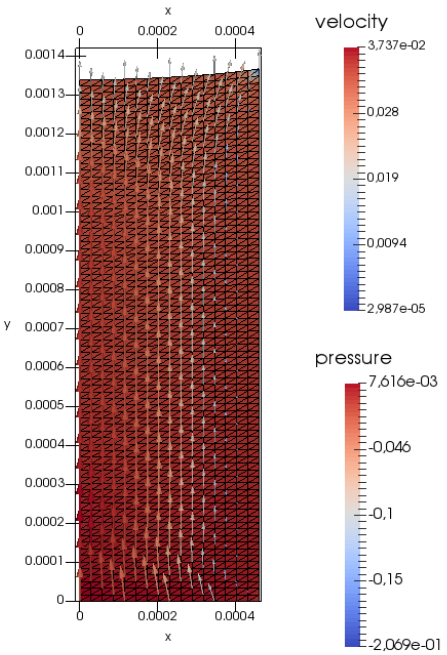

(b) $t = 0.04\,\mathrm{s}$

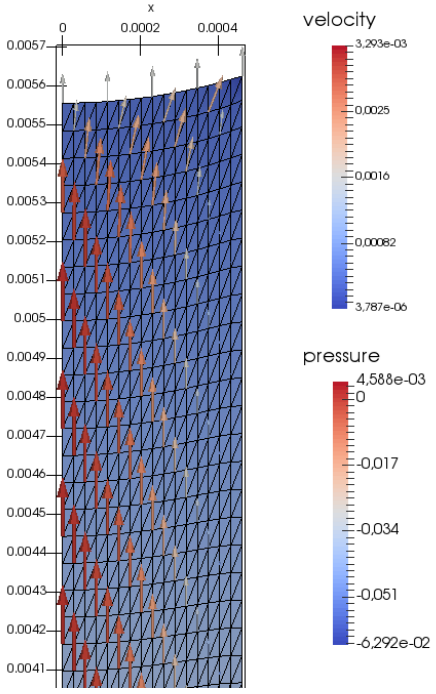

(c) $t = 1\,\mathrm{s}$

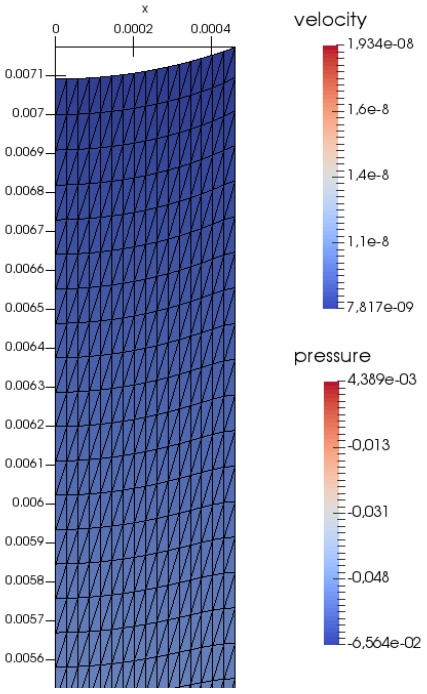

(d) $t = 6\,\mathrm{s}$

Figure 8: Evolution of domain, velocity and pressure.

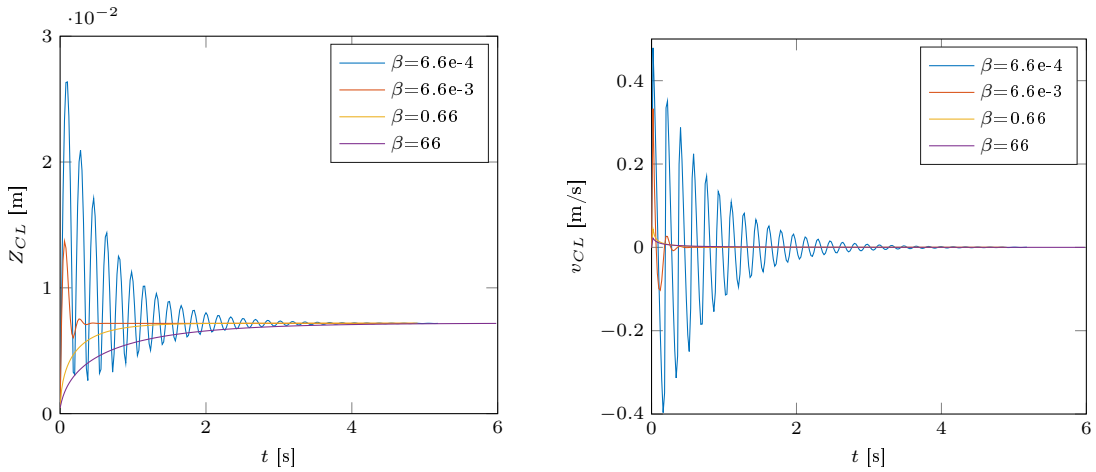

Figure 9: Contact line height (left) and fluid velocity (right) evolution for different values of β.

of the contact line height and velocity for very different values of the friction coefficient. As anticipated, a monotonic rise of the capillary height occurs if the friction is strong, whereas low values of β allow the system to oscillate around the equilibrium configuration, before achieving it. We were able to simulate very different evolutions, making β vary in a very wide range, thence we can state that our scheme is robust w.r.t. strong variations in this parameter.

Now, we move on and compare the numerical results with experimental data. Concerning the equilibrium state of the system, the results of Fig. 9 show that the final configuration is independent of the friction coefficient. This is in accordance with the established capillary action identity [21], by which the equilibrium height is determined in terms of the surface tension coefficients and the action of gravity:

$$Z_{CL}^{\infty} = \frac{2\gamma \cos\theta_s}{\rho g r},$$

where r is the radius of the capillary tube, i.e. the horizontal width of our computational domain.

In order to assess the whole time evolution of the system, in Fig. 10 we display the time-plots of the contact line height and velocity, together with the experimental observations reported in [4]: we can see a rather good agreement between the two evolutions. [7] To obtain these results, the index $1/\chi = \beta h_3$ was calibrated, as anticipated above. The outcome of our calibration is a value $\chi = 0.0095$ for the mesh-independent friction parameter, that is quite close to the value $\chi = 0.015$ employed in [4], though not completely matching it. Anyway, this discrepancy does not spoil the validity of the results, since our scheme presents some differences w.r.t. the one used in the cited work. First, we adopt a single-phase perspective, simulating only the liquid phase, whereas in [4] also the equations for the air are explicitly solved. Therefore, our parameters also condense the contributions of the gas lying above the free surface. Furthermore, a different discretization technique is employed in the cited work, and we already saw in the previous section that the discretization has a strong impact on the actual value of the friction coefficient.

So far, we have analyzed the overall dynamics of the numerical solution, focusing on the evolution of the contact line. Now we want to inspect the contributions of the various terms appearing in the balance (27), in order to understand their effects on the system. Looking at the plots of Fig. 11a-11b, it can be noticed that the main physical quantities involved in the phenomenon have comparable magnitudes. Therefore, we can infer that the physical considerations made during the derivation of the model (Sec. 3) were free of redundant attention to negligible quantities.

[7] One can notice a slight disagreement in the velocity, in the time span (0.5s, 1s). However, this non-smooth segment of the experimental data is quite probably affected by noise: indeed, it is not fitted by the numerical method in [4] either, where the data are taken from.

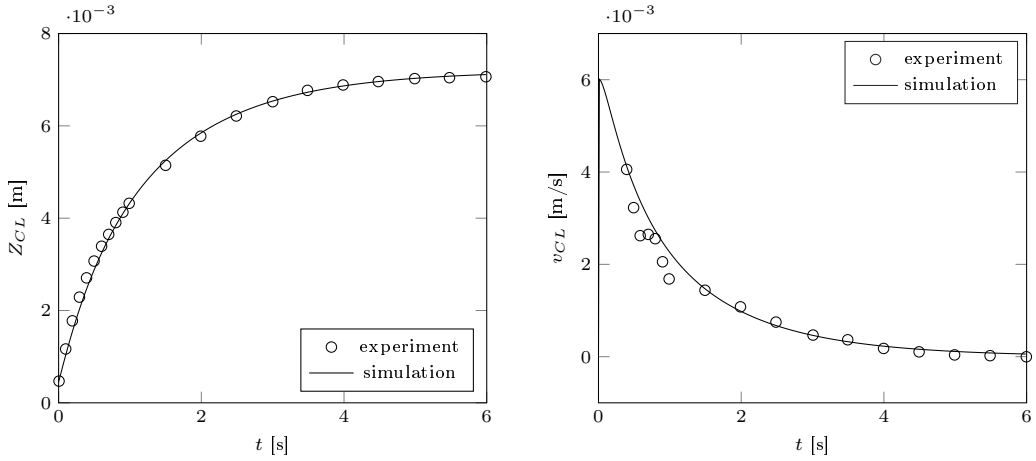

Figure 10: Height (left) and fluid velocity (right) time evolution at the contact line.

Focusing on Fig. 11b, we can observe that the purely numerical terms stemming from the implicit Euler method and the pressure stabilization are actually always positive, thus they have a dissipative effect, as expected. Anyway, such artificial contributions are quite negligible w.r.t. the overall dissipation function $\mathcal{R}^{(n+1)}$, thus they do not alter the evolution of the actual phenomenon.

A deeper comment is due on the behavior of the spurious terms, displayed in Fig. 11c. Regarding $\Phi_{expl}^{(n+1)}$ – which in principle has undetermined sign – we see that it occurs to be always positive, in the present simulation, thus not spawning any instabilizing contribution. Concerning $\varepsilon_g^{(n+1)}, \varepsilon_{\Gamma,expl}^{(n+1)}$, instead, they introduce a spurious, instabilizing power into the system, being they positive as foreseen in the remarks after Thm. 1. Yet, all these terms are at least two order of magnitudes smaller than the main terms discussed above, and hence they affect only marginally the evolution of the system.

In the results presented so far, we have shown the suitability of our scheme and its robustness w.r.t. the wall friction coefficient. Nevertheless, the situation can become troublesome if larger time steps are considered. This topic is going to be addressed in the following section.

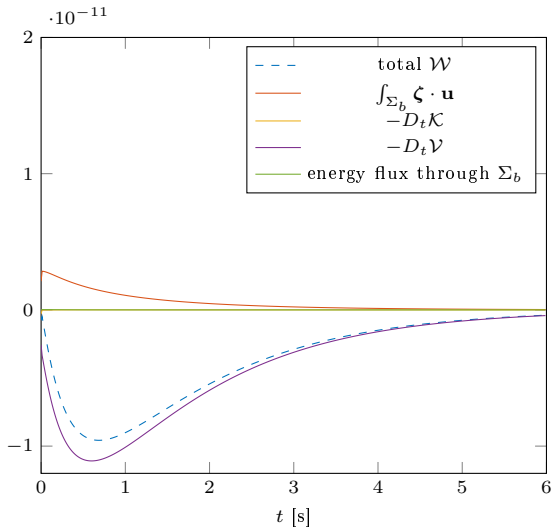

(a) Terms of the total power $\mathcal{W}$

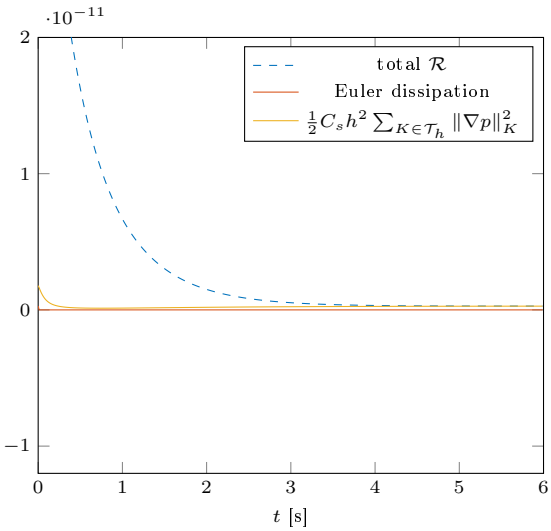

(b) Dissipative terms

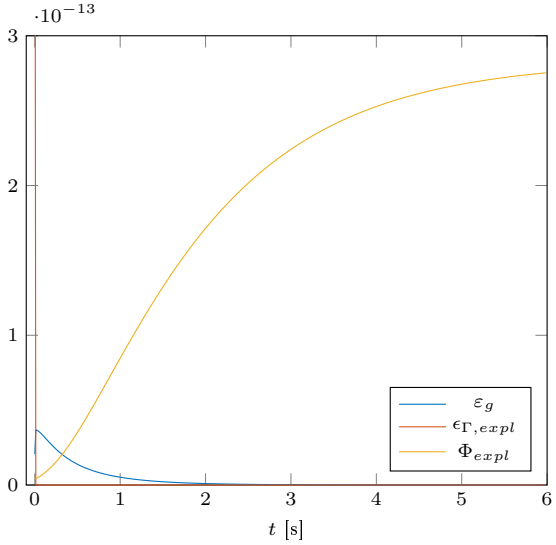

(c) Spurious terms

Figure 11: Time evolution of the terms in balance (27) ($\Delta t = 2 \cdot 10^{-5}$).

6.2.2. Effects of the stabilization term

So far we have employed a rather small time step ($\Delta t = 2 \cdot 10^{-5}$s), if compared to the physical characteristic time of the evolution we are simulating. Indeed, as one can see from Fig. 12, choosing a larger time step ($\Delta t = 4 \cdot 10^{-5}$s) is enough to make spurious oscillations appear in the velocity, pressure, and then in the geometry, after just fifteen time steps. Therefore, aiming at employing larger time steps, we need to compensate the spurious power introduced by $\varepsilon_g^{(n+1)}, \varepsilon_{\Gamma,expl}^{(n+1)}$. As anticipated in Sec. 5.1, we concentrate on the stabilization of the free surface term, by adding $S_\Gamma^{(n+1)}$ to the formulation, cf. (36). This choice is justified by the fact that the spurious oscillations displayed in Fig. 12b are mainly located on the free surface and far from the contact line. Indeed, in Fig. 12c it is possible to observe that the addition of this single term $S_\Gamma^{(n+1)}$ is sufficient to completely prevent numerical oscillations, even for large time steps.

We can find more evidence of the aptness of our stabilization by looking at how the behavior of the spurious terms $\varepsilon_g^{(n+1)}, \varepsilon_{\Gamma,expl}^{(n+1)}, \Phi_{expl}^{(n+1)}$ change for different choices of Δt, near the stability threshold $\Delta t = 2 \cdot 10^{-5}$. In Fig. 13, we focus on the first part of the time span, before the time $t = 0.001$s when the oscillations shown in Fig. 12b become too severe. As it is foreseeable, in the cases with $\alpha = 0$, all the spurious terms rapidly increase when larger time steps are chosen. However, the values of $\varepsilon_g^{(n+1)}, \Phi_{expl}^{(n+1)}$ shown in Fig. 13c remain two orders of magnitude smaller than the order of 10^{-11} of the physically consistent power terms of Fig. 11a-11b. Hence, their effect on the system is limited. On the contrary, $\varepsilon_\Gamma^{(n+1)}$ achieves much higher values in the unstabilized cases, becoming the prevailing term in the balance (27). If the stabilization is switched on by setting $\alpha = 1$ in (36), instead, this dominance is remarkably deadened (see also (37)). Indeed, in Fig. 13d we can see that the term $\Phi_S^{(n+1)}$, that basically replaces $\varepsilon_\Gamma^{(n+1)}$ when $\alpha = 1$, remains much smaller than 10^{-11}. For the sake of completeness, we point out that also the other spurious terms are brought back to the values assumed for small time steps, as one can see from Fig. 13e, so no further stabilization terms are actually needed.

As stated above, the stabilizing effect of $S_\Gamma^{(n+1)}$ can be exploited further, considering a time step $\Delta t = 2 \cdot 10^{-3}$, that is 100 times larger than the previous stability threshold, saving a significant amount of computational effort. In Fig. 14 we can see the evolution of the different terms composing the power balance (37) in such settings. Comparing them with the results of Fig. 11 (obtained with $\Delta t = 2 \cdot 10^{-5}$), practically no difference can be noticed. Indeed, our stabilization does not substantially modify the equations of the system, as it can be seen by Fig. 14c, where also the evolution of $S_\Gamma^{(n+1)}$ is shown.

Concluding this section, we want to remark that even larger time steps are actually employable without the onset of spurious oscillations. Nevertheless, choosing Δt larger than the order of milliseconds yields a major loss in accuracy, as we cannot correctly capture the fast evolution of the physical system.

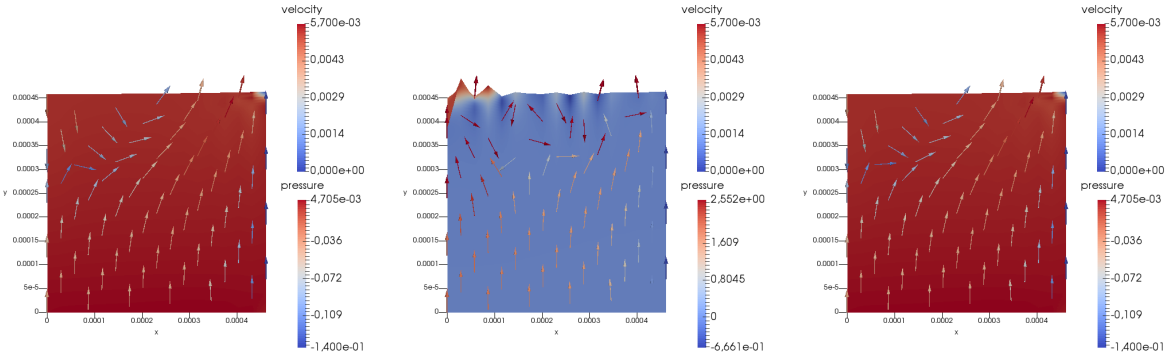

(a) $\Delta t = 2 \cdot 10^{-5}$, $\alpha = 0$: no oscillations

(b) $\Delta t = 4 \cdot 10^{-5}$, $\alpha = 0$: oscillations arise

(c) $\Delta t = 2 \cdot 10^{-3}$, $\alpha = 1$: the stabilization damps out the oscillations

Figure 12: Velocity and pressure fields at $t = 6 \cdot 10^{-4}$s. Spurious oscillations occur in the unstabilized case ($\alpha = 0$) if the time step is not small enough (b).

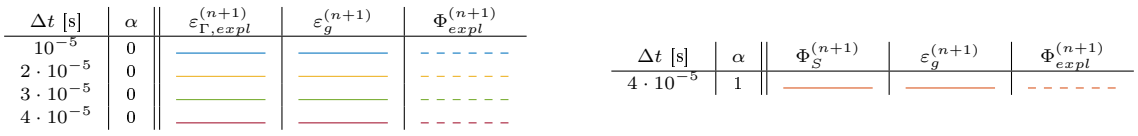

(a) Legend: values of the parameters $\Delta t, \alpha$

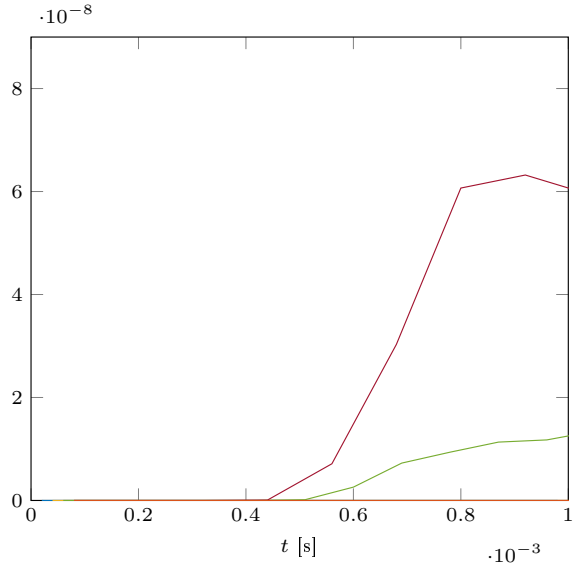

(b) $\varepsilon_{\Gamma,expl}^{(n+1)}$, $\Phi_S^{(n+1)}$

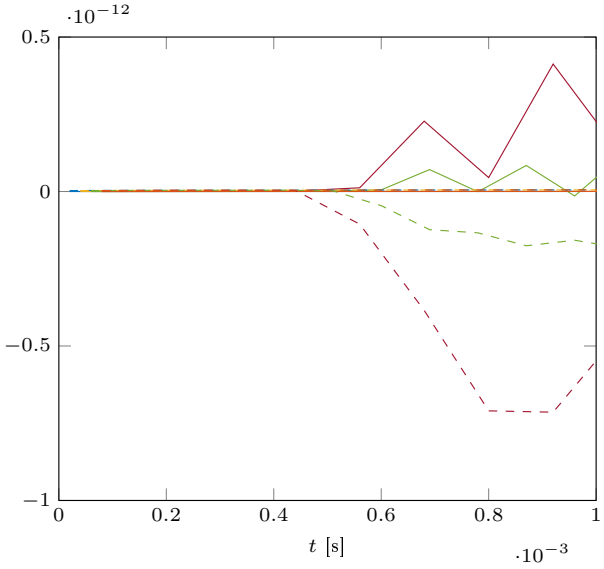

(c) $\varepsilon_g^{(n+1)}$, $\Phi_{expl}^{(n+1)}$

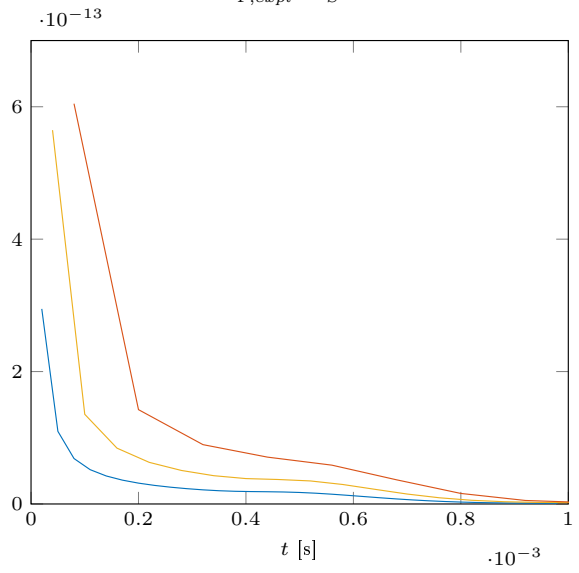

(d) $\varepsilon_{\Gamma,expl}^{(n+1)}$, $\Phi_S^{(n+1)}$

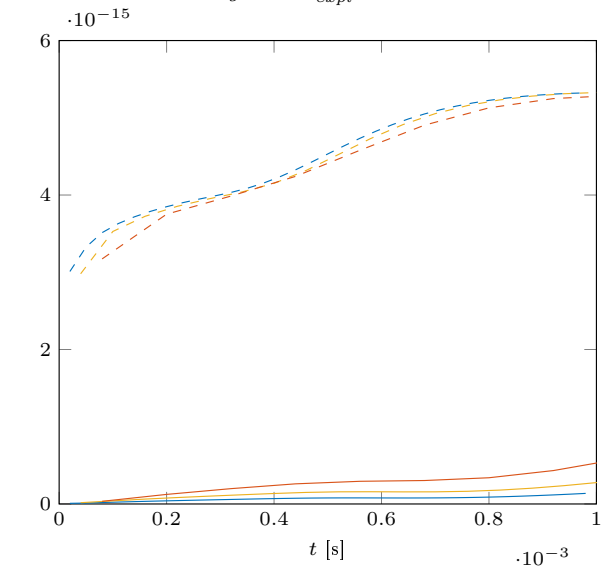

(e) $\varepsilon_g^{(n+1)}$, $\Phi_{expl}^{(n+1)}$

Figure 13: Time evolution of the spurious terms for different values of Δt near the stability threshold. In (d), (e) a zoom of (b), (c), respectively, for the cases without spurious oscillations.

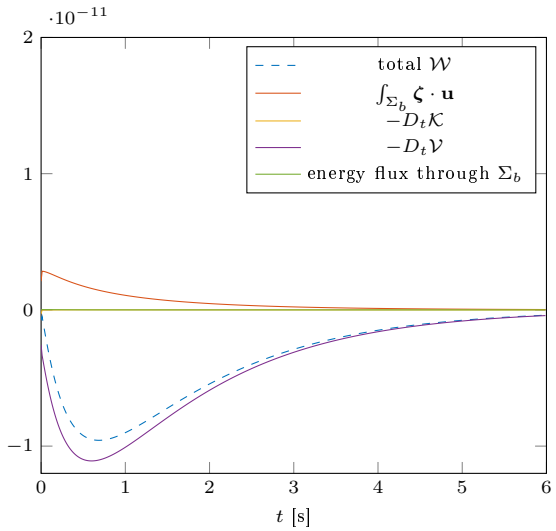

(a) Terms of the total power $\mathcal{W}$

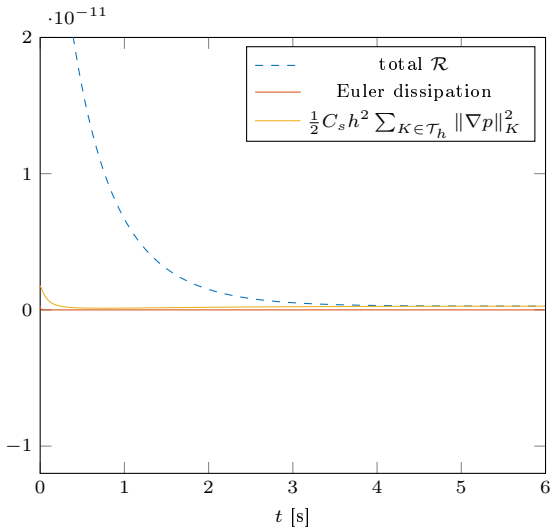

(b) Dissipative terms

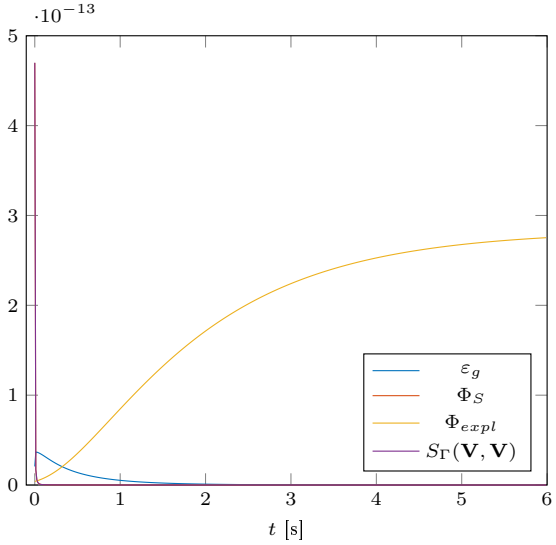

(c) Spurious terms

Figure 14: Time evolution of the terms in balance (37) with $\alpha = 1$, $\Delta t = 2 \cdot 10^{-3}$s.

7. Conclusions

In the present paper, we studied a free surface problem with moving contact line for an incompressible flow inside a capillary tube. The equations governing the phenomenon, namely Navier-Stokes equations with surface tension and wall friction, have been derived from the variational Principle of minimum reduced dissipation [20]. Such a derivation was carried out in both the cases without and with mass exchange with the environment, having both of them autonomous interest in the applications; the latter was an original extension by the authors. As a result, a physical justification of the generalized Navier boundary conditions, connecting the wall friction to the imposition of a contact angle, was given, without resorting to microscopic considerations.

Then, the stabilized $\mathbb{P}_1 - \mathbb{P}_1$ FEM discretization of the differential problem was introduced, in the Arbitrary Lagrangian-Eulerian framework, and the stability of the resulting scheme was analyzed. In particular, we investigated the ability of the numerical scheme to reproduce the First Law of Thermodynamics at the discrete level. Some purely numerical terms were isolated in the power balance of the discrete First Law, and their dissipative or instabilizing nature was determined. Then, we focused on the introduction of a novel asymptotically consistent term, aiming at correcting the discrete approximation of the surface tension power, and consequently damping the spurious instabilities that such an approximation introduces in the numerical method.

The scheme was assessed by means of different numerical tests. The mass conservation properties and the robustness of the method w.r.t. variations of physical parameters were verified. Particular attention has been paid to the wall friction coefficient and to its strong connection with the discretization parameters. The suitability of the scheme was further confirmed by the comparison with experimental results. Finally, the numerical tests demonstrated the effectiveness of the novel stabilization term in damping spurious oscillations and allowing the use of much greater time steps, yielding to significant savings in the computational effort.

Acknowledgements

The first author wants to thank the Department of Mathematics of the University of Maryland, College Park, and in particular Prof. Ricardo H. Nochetto, for hosting him for a visiting period, during which part of the present work was carried out. We thank both Prof. Nochetto and Prof. Shawn W. Walker for sharing their knowledge and expertise, that helped in the undertaking of the research summarized here. We would also like to show our gratitude to Dr. S. Turzi for his insights and the valuable discussions about the physical variational principles considered in the present work.

References

[1] J. J. W. van der Vegt, Y. Xu, Space–time discontinuous Galerkin method for nonlinear water waves, Journal of Computational Physics 224 (1) (2007) 17 – 39.

[2] L. Formaggia, E. Miglio, A. Mola, N. Parolini, Fluid–structure interaction problems in free surface flows: Application to boat dynamics, International Journal for Numerical Methods in Fluids 56 (8) (2008) 965–978.

[3] C. Bosanquet, On the flow of liquids into capillary tubes, Philosophical Magazine Series 6 45 (267) (1923) 525–531.

[4] Y. Yamamoto, T. Ito, T. Wakimoto, K. Katoh, Numerical simulations of spontaneous capillary rises with very low capillary numbers using a front-tracking method combined with generalized Navier boundary condition, International Journal of Multiphase Flow 51 (2013) 22 – 32.

[5] R. H. Nochetto, A. J. Salgado, S. W. Walker, A diffuse interface model for electrowetting with moving contact lines, Mathematical Models and Methods in Applied Sciences 24 (01) (2014) 67–111.

[6] S. W. Walker, A mixed formulation of a sharp interface model of Stokes flow with moving contact lines, ESAIM: Mathematical Modelling and Numerical Analysis 48 (4) (2014) 969–1009.

[7] A. J. Salgado, A diffuse interface fractional time-stepping technique for incompressible two-phase flows with moving contact lines, ESAIM: Mathematical Modelling and Numerical Analysis 47 (3) (2013) 743–769.

[8] C. G. Gal, M. Grasselli, A. Miranville, Cahn–Hilliard–Navier–Stokes systems with moving contact lines, Calculus of Variations and Partial Differential Equations 55 (3) (2016) 1–47.

[9] M. Sussman, P. Smereka, S. Osher, A level set approach for computing solutions to incompressible two-phase flow, Journal of Computational physics 114 (1) (1994) 146–159.

[10] S. Zahedi, K. Gustavsson, G. Kreiss, A conservative level set method for contact line dynamics, Journal of Computational Physics 228 (17) (2009) 6361–6375.

[11] C. W. Hirt, B. D. Nichols, Volume of fluid (VOF) method for the dynamics of free boundaries, Journal of Computational Physics 39 (1) (1981) 201–225.
[12] G. Tryggvason, R. Scardovelli, S. Zaleski, Direct numerical simulations of gas–liquid multiphase flows, Cambridge University Press, 2011.
[13] J. Donea, Arbitrary Lagrangian Eulerian methods, in: Computational Methods for Transient Analysis, V. 1, North-Holland, Elsevier, 1983.
[14] L. Formaggia, F. Nobile, A stability analysis for the arbitrary Lagrangian-Eulerian formulation with finite elements, East-West Journal of Numerical Mathematics 7 (2) (1999) 105–131.
[15] J.-F. Gerbeau, T. Lelièvre, Generalized Navier boundary condition and geometric conservation law for surface tension, Computer Methods in Applied Mechanics and Engineering 198 (5–8) (2009) 644 – 656.
[16] Y. D. Shikhmurzaev, Moving contact lines in liquid/liquid/solid systems, Journal of Fluid Mechanics 334 (1997) 211–249.
[17] T. Qian, X.-P. Wang, P. Sheng, Molecular hydrodynamics of the moving contact line in two-phase immiscible flows, Communications in computational physics 1 (1) (2006) 1–52.
[18] G. C. Buscaglia, R. F. Ausas, Variational formulations for surface tension, capillarity and wetting, Computer Methods in Applied Mechanics and Engineering 200 (45) (2011) 3011–3025.
[19] T. Qian, X.-P. Wang, P. Sheng, A variational approach to moving contact line hydrodynamics, Journal of Fluid Mechanics 564 (2006) 333–360.
[20] A. M. Sonnet, E. G. Virga, Dissipative ordered fluids: theories for liquid crystals, Springer Science & Business Media, 2012.
[21] G. K. Batchelor, An Introduction to Fluid Dynamics, Cambridge University Press, Cambridge, 2000.
[22] M. C. Delfour, J.-P. Zolésio, Shapes and geometries: metrics, analysis, differential calculus, and optimization, Vol. 22, SIAM, 2011.
[23] A. Laurain, S. W. Walker, Droplet footprint control, SIAM Journal on Control and Optimization 53 (2) (2015) 771–799.
[24] L. Onsager, Reciprocal relations in irreversible processes. I., Physical Review 37 (4) (1931) 405.
[25] L. Onsager, Reciprocal relations in irreversible processes. II., Physical Review 38 (12) (1931) 2265.
[26] A. Quarteroni, A. Valli, Numerical approximation of partial differential equations, Vol. 23 of Springer Series in Computational Mathematics, Springer-Verlag, Berlin, 1994.
[27] R. Temam, Navier-Stokes equations - Theory and numerical analysis, North-Holland, 1977.
[28] A. Bonito, R. H. Nochetto, M. S. Pauletti, Geometrically consistent mesh modification, SIAM Journal on Numerical Analysis 48 (5) (2010) 1877–1899.
[29] J.-F. Gerbeau, T. Lelièvre, C. L. Bris, Simulations of MHD flows with moving interfaces, Journal of Computational Physics 184 (1) (2003) 163 – 191.
[30] P. Ciarlet, The finite element method for elliptic problems, North-Holland Publishing Co., Amsterdam-New York-Oxford, 1978, studies in Mathematics and its Applications, Vol. 4.
[31] S. Brenner, R. Scott, The mathematical theory of finite element methods, Vol. 15, Springer Science & Business Media, 2007.
[32] V. Girault, P.-A. Raviart, Finite element methods for Navier–Stokes equations: theory and algorithms, Vol. 5, Springer Science & Business Media, 2012.
[33] F. Brezzi, J. Pitkäranta, On the stabilization of finite element approximations of the Stokes equations, in: Efficient solutions of elliptic systems, Springer, 1984, pp. 11–19.
[34] E. Burman, M. A. Fernández, Stabilization of explicit coupling in fluid–structure interaction involving fluid incompressibility, Computer Methods in Applied Mechanics and Engineering 198 (5) (2009) 766–784.
[35] E. Bänsch, J. Paul, A. Schmidt, An ALE finite element method for a coupled Stefan problem and Navier–Stokes equations with free capillary surface, International Journal for Numerical Methods in Fluids 71 (10) (2013) 1282–1296.
[36] M. S. Alnæs, J. Blechta, J. Hake, A. Johansson, B. Kehlet, A. Logg, C. Richardson, J. Ring, M. E. Rognes, G. N. Wells, The FEniCS project version 1.5, Archive of Numerical Software 3 (100).
URL `https://fenicsproject.org`
[37] A. Logg, G. N. Wells, J. Hake, DOLFIN: a C++/Python Finite Element Library, Springer, 2012, Ch. 10.
[38] L. F. Richardson, The approximate arithmetical solution by finite differences of physical problems involving differential equations, with an application to the stresses in a masonry dam, Philosophical Transactions of the Royal Society of London A: Mathematical, Physical and Engineering Sciences 210 (459-470) (1911) 307–357.

MOX Technical Reports, last issues

Dipartimento di Matematica
Politecnico di Milano, Via Bonardi 9 - 20133 Milano (Italy)

02/2017 Arena, M.; Calissano, A.; Vantini, S.
Monitoring Rare Categories in Sentiment and Opinion Analysis - Expo Milano 2015 on Twitter Platform.

01/2017 Riccobelli, D.; Ciarletta, P.
Rayleigh-Taylor instability in soft elastic layers

58/2016 Antonietti, P. F.; Bruggi, M. ; Scacchi, S.; Verani, M.
On the Virtual Element Method for Topology Optimization on polygonal meshes: a numerical study

56/2016 Guerciotti, B.; Vergara, C.; Ippolito, S.; Quarteroni, A.; Antona, C.; Scrofani, R.
A computational fluid-structure interaction analysis of coronary Y-grafts

57/2016 Bassi, C.; Abbà, A.; Bonaventura, L.; Valdettaro, L.
Large Eddy Simulation of gravity currents with a high order DG method

55/2016 Antonietti, P. F.; Facciola' C.; Russo A.; Verani M.;
Discontinuous Galerkin approximation of flows in fractured porous media on polytopic grids

54/2016 Vergara, C.; Le Van, D.; Quadrio, M.; Formaggia, L.; Domanin, M.
Large Eddy Simulations of blood dynamics in abdominal aortic aneurysms

52/2016 Paolucci, R.; Evangelista, L.; Mazzieri, I.; Schiappapietra, E.
The 3D Numerical Simulation of Near-Source Ground Motion during the Marsica Earthquake, Central Italy, 100 years later

53/2016 Antonietti, P. F.; Manzini, G.; Verani, M.
The fully nonconforming Virtual Element method for biharmonic problems

51/2016 Guzzetti, S.; Perotto, S.; Veneziani, A.
Hierarchical Model Reduction for Incompressible Flows in Cylindrical Domains: The Axisymmetric Case